Effects of wind trend and gustiness on the sea drag: Lake George study

Alexander V. Babanin[1] and Vladimir K. Makin[2]

Received 21 March 2007; revised 8 September 2007; accepted 7 November 2007; published 19 February 2008.

[1] The air-sea coupling is usually parameterized in terms of the drag coefficient C_d, but the scatter of experimental data around such dependences is very significant and has not improved noticeably over some 30 years. In the paper, which is meant to be the first in a series, a complex approach to the problem is suggested. Multiple mechanisms, contributing into the sea drag, are to be singled out, studied separately, evaluated and then reunited in a joint parameterization for C_d. Dependences of the drag coefficient on the wind speed and sea state, and effects of wind trends and gustiness are investigated in detail. Gustiness is found to be responsible for the most distant outliers. Our approach also combines an experimental Lake George study with theoretical investigations conducted by means of the WOWC (Wind-Over-Waves Coupling) model. Overall agreement of the model with measured wind stresses is quite good, within 20% for the bulk of the data. Lower envelopes of the drag dependences are an important result of the paper. They provide some Lake George "ideal" relationships for the sea drag. Almost any deviation from such conditions causes the drag to increase. It is suggested that decrease of the drag with respect to the ideal conditions, which exhibits itself in a number of known open ocean data sets, would be caused by a momentum flux back from the waves to the wind due to long waves outrunning the wind. Behavior of the Charnock parameter in terms of wave age is also considered.

Citation: Babanin, A. V., and V. K. Makin (2008), Effects of wind trend and gustiness on the sea drag: Lake George study, *J. Geophys. Res.*, *113*, C02015, doi:10.1029/2007JC004233.

1. Introduction

[2] Understanding of the coupling between the atmosphere and the ocean surface is important for many scientific, environmental and engineering problems. These include predictions of climate change, operational and extreme wind and wave properties, atmospheric and oceanic circulation, remote sensing techniques. Accurate predictions of these quantities are of fundamental importance to meteorologists, coastal and ocean engineers, climate researchers, shipping companies, the offshore oil and gas industry and coastal planners, among others.

[3] Coupling between the atmospheric boundary layer and the ocean surface is usually parameterized in terms of the drag coefficient C_d

$$\tau = \rho_a u_*^2 = \rho_a C_d U_{10}^2 \tag{1}$$

where τ is the wind stress at the ocean surface, ρ_a is the density of air, U_{10} is the wind speed measured at a reference height of 10m and u_* is the friction velocity. Equation (1) relies on the concept of constant-flux layer, i.e., on existence of a bottom part of the atmospheric boundary layer where combined viscous-turbulent friction force dominates all the other possible forces. This concept proved very consistent in general fluid mechanics when constant-speed flows over solid walls are considered. In case of ocean waves, evolving simultaneously at multiple timescales, from very long and continuous (slow growth due to wind input and non-linear interactions) through to very short (wave breaking), with their very complex physics and multiple mechanism for imparting feedback on the atmospheric flow, deviations from the assumed simple friction forcing can be expected, particularly as the winds are ever changing and gusty too. Besides, at low wind speeds, the height of this layer can be less than 10 m [e.g., *Komen*, 1994], and equation (1) would not be valid. When applicable, however, knowledge of C_d enables a simple determination of the wind stress or the flux of momentum from the wind to the waves, if U_{10} is specified.

[4] Accurate evaluation of C_d has proven to be a major challenge since it requires precise field measurements of fine turbulent fluctuations in the atmospheric boundary layer close to the wavy surface. The available field data has resulted in a number of quite different parameterizations [*Young*, 1999]. Routinely, C_d is parameterized as a function of mean wind speed U_{10}, but the scatter of experimental data around such parametric dependences is very significant and has not improved noticeably over

[1] Faculty of Engineering and Industrial Sciences, Swinburne University of Technology, Melbourne, Victoria, Australia.
[2] Royal Netherlands Meteorological Institute (KNMI), De Bilt, Netherlands.

0148-0227/08/2007JC004233

some 30 years. This scatter imposes a serious limitation on forecasts and predictions that make use of sea surface drag parameterizations.

[5] Also, since measuring C_d in extreme wind and wave conditions is logistically particularly difficult, the majority of the data has been obtained during light to moderate winds. This, in addition to the scatter, further limits applicability of the available parameterizations because their extrapolation into extreme conditions is questionable. Different physics is expected to drive air-sea interaction at very strong wind-forcing conditions as has been shown in an escalating series of recent studies [*Powel et al.*, 2003; *Donelan et al.*, 2004, 2006; *Makin*, 2005; *Bye and Jenkins*, 2006; *Kudryavtsev*, 2006; *Kudryavtsev and Makin*, 2007; *Vakhguelt*, 2007]. This limitation is particularly important for modeling extreme events, such as tropical cyclones, and also for long-term climate prognosis, which predicts increasing frequency of such events. It is felt, however, even at moderate-wind conditions as some parts of the continuous wave spectrum are always subject to strong forcing and thus further contribute to uncertainties and scatter of C_d estimates [*Donelan et al.*, 2006; *Kudryavtsev and Makin*, 2007].

[6] Parameterizing C_d in terms of mean wind speed U_{10} bears further deficiencies. The mean wind speed U_{10} do not define the wave properties, like mean or dominant wave height and length, even for ideal wave development situations. Depending on duration of the wind action and on wave fetch, the waves will evolve from short young seas into much longer old seas. Young waves are on average much steeper compared to the old ones, and most of other wave characteristics evolve too. This is known as the sea state dependence, with U/c_p usually being the sea state (or inverse wave age) parameter where c_p is the phase speed of waves at the wave spectrum peak. A sea state dependence in C_d has long been foreshadowed [e.g., *Stewart*, 1974], but only relatively recently has it been observed in field measurements. Some support has been found in a number of data sets [e.g., *Smith et al.*, 1992; *Donelan et al.*, 1993; *Oost et al.*, 2001; *Drennan et al.*, 2003, among others], but notably not in others [e.g., *Yelland et al.*, 1998]. A recent effort at reconciling this fundamental issue has been on the basis of the dominant wave steepness [e.g., *Taylor and Yelland*, 2001; *Oost et al.*, 2001]. However, the dominant sea waves are known to play a relatively small direct role in determining the wind stress, except possibly for very young wind seas. Unless the waves are young, dominant waves are fast and their interaction with the wind is weak, but the effect of the dominant waves on sea drag may be indirect – by means of modulating the shorter waves [*Kudryavtsev and Makin*, 2002; *Hara and Belcher*, 2002] or due to airflow separation from breaking dominant waves [*Makin and Kudryavtsev*, 2002]. This highlights the need to understand more completely the basic physics of the sea surface wind stress in order to parameterize it reliably in the form of a drag coefficient.

[7] Many other effects can contribute significantly to the wind stress. Gustiness of the wind, which is always a feature of real wind fields, is accommodated in a number of theories [*Janssen*, 1986; *Miles and Ierley*, 1998] and may result in either reduction of the stress or its enhancement. The winds and waves are also non-stationary, which has been shown to have a major effect on estimating the wind input. *Uz et al.* [2002] concluded that the wind stress tends to be higher in decreasing winds than with increasing winds at a given wind speed, mainly due to delayed response of the short waves to varying wind-forcing. *Skafel and Donelan* [1997] demonstrated modulation of the wind stress by the passage of wave groups. *Makin* [1988] and *Agnon et al.* [2005] found wind-input oscillations due to non-linear wind-wave interactions.

[8] Another uncertain source of potentially significant stress variations is the swell present on the ocean surface. *Dobson et al.* [1994] did not find noticeable influence of the swell on the sea drag, whereas *Donelan et al.* [1997], *Drennan et al.* [1999], and *Guo-Larsen et al.* [2003] revealed significantly enhanced drag coefficients for cross-wind and, particularly, for adverse-to-the-wind swell. These features of swell were theoretically explained by *Kudryavtsev and Makin* [2004]. *Smedman et al.* [1999], *Drennan et al.* [1999] and *Grachev et al.* [2003] observed negative stress (momentum flux from the waves to the wind) for swell following the wind. Potentially, swell can influence the dominant and short wind wave spectra through hydrodynamic interactions, and through the interaction of the changed spectra with the wind – the sea drag. However, we are not aware of any measurements of such kind in the field. The interaction of long paddle waves (erroneously referred to as swell) with the short wind-induced waves and the wind in the laboratory conditions has different physics as discussed by *Makin et al.* [2007]. In any case, swell does not exist in Lake George and so we will not be concerned with this issue in the present paper.

[9] This short review emphasizes the need for a complex approach to account for multiple phenomena that may simultaneously affect the sea drag. The recent Lake George field measurements elucidated many issues mentioned above and highlighted others. The Lake George data in combination with the wind-over-waves coupled (WOWC) approach outlined below enable us to address effectively, with obvious limitations, the complex processes associated with small-scale air-sea interaction, and therefore the sea drag.

[10] We believe that a complete list of physical properties and phenomena, whose effect on the sea drag should be investigated and incorporated in the final parameterization to reduce the scatter, includes, among possible others, 1) mean wind speed; 2) sea state dependence; 3) wave steepness; 4) full flow separation for strongly forced wind waves; 5) enhancement of sea drag due to wave breaking; 6) rising and falling winds; 7) gustiness of the wind; 8) temperature stratification in the atmospheric boundary layer; 9) swell; 10) non-linear wind-wave interactions; 11) wave horizontal skewness and vertical asymmetry; 12) variation of the wavy surface properties at wave group and wavelength scales; 13) wave directionality; 14) wave short-crestedness; 15) coupled effects in the air/sea boundary layers. The 16th and separate item would be that due to peculiarities of air-sea interaction at extreme wind-forcing conditions which include an entire set of new features irrelevant at moderate winds as mentioned above. In this list, we do not mention properties and processes which breach validity of the constant-flux-layer approximation, as in such circumstances the notion of the drag coefficient (1) becomes

Table 1. Lake George Data Used for the Analysis[a]

No.	Rec. No.	U_{10}, m/s	Direction, degrees	f_p, Hz	Depth, m	Gustiness G	Trend, T (m/s)/min	Gustiness Detrended $G_{detrended}$	u_*, m/s	H_s, m	$C_d \cdot 10^3$
1	151249	9.9	288	0.42	1.10	0.08	−0.07	0.06	0.36	0.31	1.32
2	151318	9.4	307	0.42	1.10	0.13	0.16	0.09	0.35	0.26	1.39
3	151342	9.1	297	0.46	1.10	0.07	−0.08	0.05	0.33	0.27	1.32
4	151410	9.7	290	0.44	1.10	0.07	0.02	0.07	0.33	0.29	1.16
5	031211	13.7	290	0.37	1.15	0.05	−0.03	0.05	0.54	0.38	1.55
6	031233	13.6	294	0.39	1.15	0.04	−0.04	0.04	0.54	0.35	1.58
7	031253	13.4	297	0.39	1.15	0.05	−0.06	0.05	0.54	0.36	1.62
8	031310	12.6	289	0.39	1.15	0.05	0	0.05	0.46	0.35	1.33
9	031327	13.2	289	0.39	1.15	0.06	−0.07	0.06	0.51	0.36	1.49
10	031347	12.8	290	0.39	1.15	0.10	0.11	0.09	0.48	0.33	1.41
11	031407	13.9	299	0.37	1.15	0.05	0.06	0.05	0.55	0.37	1.57
12	031427	13.4	290	0.39	1.15	0.06	−0.04	0.06	0.52	0.36	1.51
13	111051	12.9	284	0.63	1.14	0.09	−0.04	0.09	0.57	0.24	1.95
14	111156	12.6	283	0.61	1.14	0.08	−0.01	0.08	0.55	0.25	1.91
15	111224	11.9	278	0.61	1.14	0.09	0.01	0.09	0.50	0.23	1.77
16	111402	13.0	278	0.59	1.14	0.08	−0.01	0.08	0.56	0.25	1.86
17	111538	11.6	280	0.66	1.14	0.07	0.05	0.06	0.48	0.22	1.71
18	141250	11.0	291	0.73	1.09	0.08	0.02	0.07	0.45	0.18	1.67
19	141215	10.1	288	0.75	1.09	0.08	0.06	0.05	0.39	0.16	1.49
20	161454	9.8	274	0.73	1.04	0.08	−0.04	0.07	0.38	0.16	1.50
21	271100	6.1	297	0.51	0.95	0.14	0.01	0.14	0.28	0.17	2.11
22	271235	7.8	286	0.51	0.95	0.13	0	0.13	0.34	0.20	1.90
23	281544	5.1	293	0.59	0.96	0.17	−0.13	0.07	0.16	0.14	0.98
24	311638	9.3	326	0.51	0.94	0.10	0.09	0.09	0.44	0.17	2.24
25	311702	9.3	330	0.46	0.94	0.14	−0.2	0.06	0.40	0.19	1.85
26	311731	10.0	338	0.81	0.94	0.11	0.05	0.10	0.41	0.19	1.68
27	311757	17.1	272	0.41	1.12	0.11	−0.22	0.08	0.75	0.34	1.92
28	311823	19.8	273	0.37	1.12	0.09	−0.21	0.07	0.98	0.46	2.45
29	311845	15.0	275	0.32	1.04	0.06	0.01	0.06	0.63	0.41	1.76
30	311908	12.9	282	0.34	0.93	0.08	−0.13	0.06	0.53	0.37	1.69
31	311930	12.8	285	0.39	0.95	0.05	0.02	0.05	0.52	0.32	1.65
32	311958	11.6	285	0.39	0.99	0.07	−0.03	0.07	0.43	0.31	1.37
33	312021	13.7	289	0.42	1.02	0.05	0.01	0.05	0.57	0.35	1.73
34	312048	13.2	298	0.38	1.02	0.08	−0.08	0.07	0.55	0.35	1.74
35	312111	9.3	305	0.39	0.86	0.07	0.01	0.07	0.35	0.25	1.42
36	312207	8.6	311	0.46	0.85	0.04	0	0.04	0.30	0.20	1.22
37	312232	9.0	310	0.49	0.86	0.06	0.04	0.05	0.33	0.21	1.34
38	312254	9.1	320	0.46	0.88	0.07	−0.01	0.07	0.34	0.22	1.40
39	312316	8.5	319	0.46	0.87	0.06	0.03	0.05	0.31	0.20	1.33
40	312339	8.6	320	0.49	0.88	0.05	−0.04	0.05	0.31	0.20	1.30
41	010004	9.9	318	0.54	0.86	0.05	0.04	0.05	0.38	0.21	1.47
42	010030	10.7	317	0.46	0.87	0.07	0.11	0.04	0.43	0.23	1.61
43	010055	11.8	318	0.46	0.87	0.04	0	0.04	0.51	0.25	1.87
44	010118	12.1	316	0.44	0.84	0.04	−0.02	0.04	0.52	0.25	1.85
45	010140	12.6	301	0.42	0.87	0.06	0.07	0.05	0.55	0.28	1.91
46	010204	13.4	296	0.39	0.89	0.07	0.06	0.06	0.61	0.31	2.07
47	010226	13.9	294	0.39	0.9	0.07	0.11	0.05	0.62	0.34	1.99
48	010248	14.8	291	0.39	0.93	0.06	0.01	0.06	0.67	0.36	2.05
49	010716	11.7	289	0.39	1.07	0.07	0	0.07	0.43	0.29	1.35
50	010739	12.1	285	0.39	1.08	0.09	−0.06	0.08	0.46	0.31	1.45
51	010803	13.1	286	0.41	1.06	0.09	0.12	0.07	0.50	0.30	1.46
52	010827	13.2	289	0.39	1.08	0.06	−0.05	0.05	0.51	0.30	1.49
53	010849	11.9	282	0.41	1.07	0.07	0.07	0.06	0.44	0.30	1.37
54	141237	12.0	286	0.37	0.98	0.11	0.15	0.07	0.51	0.28	1.81
55	141305	14.1	286	0.37	1.00	0.11	0.18	0.08	0.64	0.31	2.06
56	141328	14.3	279	0.37	1.02	0.07	−0.09	0.06	0.62	0.32	1.88
57	141351	14.5	278	0.34	1.04	0.07	0.01	0.07	0.62	0.34	1.83
58	141415	15.5	282	0.34	1.05	0.08	0.14	0.06	0.69	0.32	1.98
59	201446	6.7	277	1.05	0.89	0.16	−0.11	0.13	0.26	0.093	1.51
60	201532	5.6	276	1.00	0.89	0.10	0	0.10	0.22	0.078	1.54
61	261148	5.9	277	0.93	0.84	0.18	0.06	0.15	0.28	0.079	2.25
62	261219	7.2	285	0.56	0.84	0.13	0.03	0.13	0.40	0.097	3.09
63	261330	8.1	261	0.54	0.84	0.11	−0.08	0.09	0.35	0.11	1.87
64	041137	4.3	286	0.82	0.76	0.21	0.02	0.21	0.13	0.098	0.91
65	151238	11.1	275	0.49	0.82	0.09	0.04	0.09	0.41	0.19	1.36
66	151301	11.8	274	0.46	0.84	0.07	−0.03	0.06	0.45	0.22	1.45
67	151325	11.8	275	0.44	0.85	0.11	−0.01	0.11	0.45	0.22	1.45
68	161425	6.9	286	0.95	0.71	0.11	−0.01	0.11	0.26	0.09	1.42
69	161507	7.1	287	1.14	0.70	0.14	−0.07	0.14	0.29	0.09	1.67
70	221253	9.8	286	0.38	0.70	0.10	0.03	0.10	0.38	0.15	1.50
71	221421	9.5	274	0.33	0.71	0.13	0.06	0.12	0.33	0.15	1.21
72[a]	8	11.9	285	0.54	0.32	-	-	-	0.44	0.156	1.37

Table 1. (continued)

No.	Rec. No.	U_{10}, m/s	Direction, degrees	f_p, Hz	Depth, m	Gustiness G	Trend, T (m/s)/min	Gustiness Detrended $G_{detrended}$	u_*, m/s	H_s, m	$C_d \cdot 10^3$
73[a]	9	12.0	288	0.55	0.28	-	-	-	0.45	0.134	1.41
74[a]	11	10.6	281	0.57	0.32	-	-	-	0.36	0.078	1.15

[a]Indicates records for which parameters of gustiness and mean trend were not estimated. Friction velocity u_* is that obtained from the anemometer mast measurements of mean wind profile.

uncertain. Since a significant number of large-scale processes in the atmosphere disrupt the constant-flux physics, parameterizations for the drag coefficient are bound to have some residual scatter.

[11] Properties 13) and 14) have not so far been shown to affect the sea drag, but we believe they do. For example, for short-crested waves, the airflow has a possibility to skirt around the crests, which should reduce the surface resistance compared to the long-crest situation.

[12] The approach combines an experimental study with theoretical investigations conducted by means of the WOWC model. Experiment, although is an ultimate truth, is hardly able to separate effects of the multiple influences listed above. This can be done within the WOWC model, by switching on and off different physical mechanisms. If, for particular conditions, the experiment and the model produce identical or close results, we assume that physics included in the model is adequate for the relevant field circumstances. If, on the contrary, there are essential discrepancies between the measurement and the model, such cases will be scrutinized to find the cause.

[13] The present paper considers behavior of C_d in terms of wind speed U_{10} and sea state U/c_p and is mainly dedicated to the effects that the rising and falling winds 6) and gustiness 7) have on the C_d parameterizations. The latter effects were found to be the major source of disagreement between our experiment and our model.

2. The Experiment

[14] The Lake George finite-depth field experiment is well-documented in literature and we refer to *Young et al.* [2005] for the most complete and detailed summary. Here, we will only mention that the aim of the Lake George project was to simultaneously measure source/sink functions, as well as fetch-limited wave evolution. An integrated set of instruments was deployed in all four relevant environments: the atmospheric boundary layer, the water surface, the water column and the bottom boundary layer. All measurements were synchronized and many of them were intentionally redundant in order to provide means for cross-checks, consistency verifications and balance closures [e.g., *Babanin et al.*, 2005].

[15] The waves were recorded with a stationary directional eight-probe wave array and by a set of mobile one-probe arrays which were used to record short-scale spatial variability of wave trains. Detection of breaking events was also carried out by multiple means [*Babanin et al.*, 2001].

[16] In this paper we are mainly interested in the air-side boundary layer observations. The wind profile was obtained by means of the anemometer mast with 6 cup anemometers logarithmically spaced from 10m height down to 22 cm above the mean sea level. The wind directions were measured at 10-m and 0.89-m heights. The wind probes were Aanderaa Instruments Wind Speed Sensors 2740 and Wind Direction Sensors 3590. The speed sensor provided 1-min average wind speeds and gusts. Accuracy of the wind speed measurements is ±2% or 0.2 *m/s* whichever is greater.

[17] For redundancy in the wind speed and momentum flux estimates, a Gill Instruments Ultrasonic Anemometer was also deployed on the mast and sampled the three-dimensional air velocity at 21 Hz rate. During the 3-year observational period, this instrument was once shipped to the manufacturer to check its calibration characteristics and therefore the sonic measurements do not cover the entire experiment duration while the profile measurements do.

[18] Records analyzed in the present paper were mostly taken during the first year of observations and their relevant characteristics are summarized in Table 1. The water depth during this year stayed close to 1 m.

[19] Capability of the Lake George anemometer-mast measurements is demonstrated in Figure 1. In the top panel, profiles of the near-surface winds are shown for records of mean U_{10} wind conveniently separated by 5 m/s: 5.1, 10.0, 15.0, and 19.8 m/s (records 281544, 311731, 311823, 311845 from Table 1). No significant or systematic deviations from the logarithmic profile are evident. Overall, correlation coefficients for the logarithmic profiles employed were above 99%. Therefore stratification effects will not be considered in the present paper. In any scenario they are expected to be insignificant as air-water temperature differences in the 1-m deep Lake George were usually small, within a few degrees, with water temperature of the shallow lake fast-tracking any atmospheric changes.

[20] Wind unsteadiness, particularly the gustiness, was on the contrary found to have played a major role in altering the boundary layer fluxes and contributing to the drag coefficient scatter. Therefore these features will be investigated in most detail in the paper. In the bottom panel, one-minute average wind speeds at the 10 m height for the four records are shown.

[21] The mean trend T is further defined as the slope of the linear regression between these 1-min averages and time t in minutes:

$$U_{10}(t) = T \cdot t + B \tag{2}$$

where B is intersect.

[22] The gustiness is defined as

$$G = std(U_{10})/mean(U_{10}) \tag{3}$$

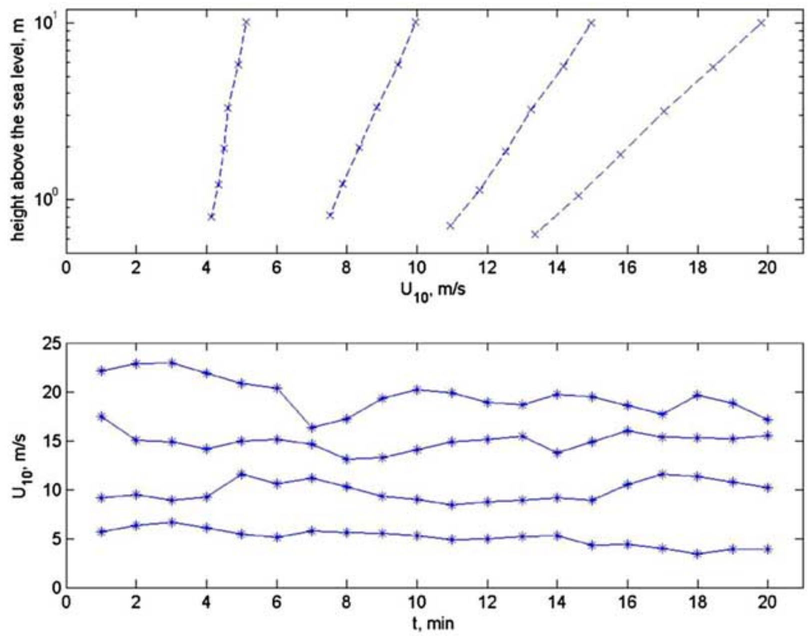

Figure 1. (*top panel*) 20-min average measured wind profiles for wind speeds of U_{10} = 5.1, 10.0, 15.0, and 19.8 m/s consequently. (*bottom panel*) One-minute average wind speeds at the 10 m height for these records. The records are 281544, 311731, 311823, 311845 from Table 1.

and has two entries in this paper: G calculated for the original 1-min wind time series and $G_{detrended}$ calculated after the mean trend has been removed.

[23] In Figure 1, bottom panel, the lightest and strongest winds exhibit the largest negative trend T of -0.13 $\frac{m}{s}$/min and -0.21 $\frac{m}{s}$/min respectively. The latter is the second largest trend in the entire data set. Mean trends for the two intermediate winds are small: T = 0.05 $\frac{m}{s}$/min and 0.01 $\frac{m}{s}$/min, the last one being negligible.

[24] Gustiness is the largest for the lightest wind and smallest for the strongest winds, as it is generally the case. For all but 10m/s winds in Figure 1, the detrended gustiness is below the value of $G_{detrended}$ = 0.09 which is set as a data quality-control threshold in section 6 below. A very significant difference between gustiness G and gustiness detrended $G_{detrended}$ for the 5 m/s record should be pointed out: 0.17 and 0.07 respectively. It is also worth noticing that the wind trend and gustiness do not necessarily correlate: the largest wind trend of T = -0.21 at 20m/s wind is accompanied by a below-the-threshold gustiness of G = 0.09 and $G_{detrended}$ = 0.07 whereas the small wind trend T = 0.05 of the 10m/s record corresponds to an above-the-threshold gustiness of G = 0.11 and $G_{detrended}$ = 0.10.

[25] The selection of records in Figure 1, therefore, illustrates a wide variety of small-scale wind unsteadiness. This does not appear to cause deviations from the logarithmic boundary layer wind profile, but have a potential to affect sea drag in a serious way as will be shown below.

[26] The logarithmic profile

$$u(z) = \frac{u_*}{\kappa} \ln \frac{z}{z_0} \tag{4}$$

is the solution of the horizontal momentum equations for the near-surface boundary sublayer dominated by friction forces, both viscous and turbulent [e.g., *Komen*, 1994]:

$$\partial\tau/\partial z = 0. \tag{5}$$

[27] In this sublayer, therefore, vertical momentum flux (wind stress) τ does not depend on height z (the constant-flux layer). Above, z_0 is the characteristic length of surface roughness and κ is the von Karman constant.

[28] The friction velocity u_* obtained from the wind profiles (4) can also be measured using the sonic anemometer:

$$u_*^2 = \overline{-U'w'} \tag{6}$$

where U' and w' are oscillations of the horizontal (i.e., length of vector sum of the down-wind and cross-wind components) and vertical velocities, correspondingly. Thus the constancy of τ and adequacy of the wind profile measurements, can be verified.

[29] In Figure 2, u_* measurements by the sonic anemometer (u_{*sonic}) and by the anemometer mast ($u_{*profile}$) are compared (corresponding data are tabulated in Table 2). As seen in the left panel of u_{*sonic} versus $u_{*profile}$, the scatter is significant, but overall matching in terms of absolute values of u_* is satisfactory, with correlation coefficient of 95% and sampling standard deviation of 0.06m/s.

[30] Right panel, however, identifies a potential problem. In this subplot, ratio of u_{*sonic} and $u_{*profile}$ is plotted versus U_{10}. At the low U_{10} wind speeds, the ratio can be as large as 3. This considerable scatter of the relative values of u_* shows that assumption of the constant-flux layer could have been violated by background processes in the atmosphere

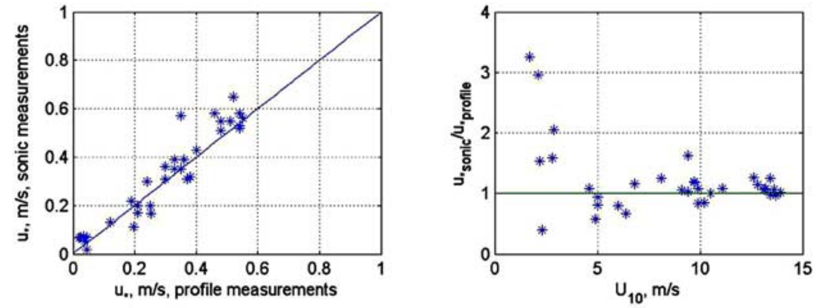

Figure 2. Comparison of friction velocity u_* obtained by means of stress measurements (sonic anemometer) and measurements of the mean wind profile in the boundary layer (vertical array of cup anemometers). (*left panel*) u_{*sonic} versus $u_{*profile}$. (*right panel*) Ratio of u_{*sonic} and $u_{*profile}$ versus U_{10}.

and at U_{10} < 4 m/s the concept of the constant flux may not be valid over the ocean as described by *Komen* [1994]. This can be due to non-stationarity and non-homogeneity of the mean wind, which is very likely for fields of light winds, or perhaps height of the constant-flux layer can be less than 10m as mentioned in Introduction. On the other hand, as was pointed out by our Reviewer, ''the expectation value of the ratio $E[\frac{u_*+noise_{sonic}}{u_*+noise_{profile}}]$ would usually tend to a large value as $u_* \rightarrow 0$ for most reasonably behaved random noise distributions'' since the random noise of the sonic-anemometer measurements is obviously higher. In any case, the light-wind records were excluded from our analysis as it is routinely done by all other researchers, and in our case U_{10} = 4 m/s was chosen as the cut-off speed. Reduction of the scatter toward higher wind speeds is apparent, and for U_{10} > 4 m/s the constant-flux concept can certainly be applied.

3. The WOWC Model

[31] Wind-over-waves coupling (WOWC) is a modern theory of microscale air-sea interaction, which allows to relate the sea drag (surface stress) directly to the properties of wind waves and peculiarities of their interaction with the wind. The advanced WOWC theory/model was developed in the last decade by *Makin et al.* [1995], *Makin and Kudryavtsev* [1999, 2002], *Kudryavtsev et al.* [1999], and *Kudryavtsev and Makin* [2001]. The WOWC model is based on the conservation equation for integral momentum, which relates the friction velocity to the sea surface stress (sea drag). It preassumes stationary and spatial homogeneous conditions for the wave and wind fields. Such non-stationary features of the wind field as the wind trend and gustiness, though could be in principle introduced into the model, are not accounted for in the present version. Further, it is assumed that the wind direction coincides with the mean direction of wave propagation and the wave spectrum is symmetrical relative to that direction, the situation typical for the Lake George.

[32] The surface stress is supported by viscous stress and the form drag, the latter being the correlation of the wave-induced pressure field with the wave slope. The form drag is supported by the wave-induced stress described in term of the non-separated sheltering mechanism [e.g., *Belcher and Hunt*, 1993], and by stress due to separation of the airflow from breaking wind waves. The latter is further split up into the separation stress supported by short gravity waves in the equilibrium range of the wave spectrum, and the separation stress supported by dominant (waves in the spectral peak of a wind wave spectrum) waves. The theory provides a clear understanding of the physical mechanisms forming the surface stress, and an explanation on what causes the stress

Table 2. Comparison of Friction Velocity u_* Measured by the Vertical Array of Wave Probes ($u^*_{profile}$) and by the Sonic Anemometer (u^*_{sonic})[a]

No.	Rec. No.	U_{10}	$u^*_{profile}$	u^*_{sonic}
1	151249	9.9	0.36	0.39
2	151318	9.4	0.35	0.57
3	151342	9.1	0.33	0.35
4	151410	9.7	0.33	0.39
5	031211	13.7	0.54	0.52
6	031233	13.6	0.54	0.58
7	031253	13.4	0.54	0.53
8	031310	12.6	0.46	0.58
9	031327	13.2	0.51	0.55
10	031347	12.8	0.48	0.55
11	031407	13.9	0.55	0.56
12	031427	13.4	0.52	0.65
13	281153	6.0	0.25	0.20
14	281234	5.0	0.21	0.17
15	011245	9.9	0.37	0.31
16	011323	10.2	0.38	0.32
17	011406	11.1	0.40	0.43
18	011445	13.1	0.48	0.51
19	191134	9.4	0.30	0.31
20	191214	10.5	0.35	0.35
21	191348	9.7	0.30	0.36
22	211132	4.6	0.12	0.13
23	211202	6.8	0.19	0.22
24	211320	8.1	0.24	0.30
25	081259	2.2	0.036	0.055
26	281335	5.0	0.211	0.198
27	031105	4.9	0.198	0.113
28	221115	6.4	0.254	0.168
29	041117	2.8	0.044	0.07
30	281133	2.9	0.035	0.072
31	281308	2.3	0.045	0.018
32	081405	1.7	0.020	0.065
33	081435	2.1	0.024	0.071

[a]Units of all wind speeds are m/s. The first 12 records are the same as those in Table 1.

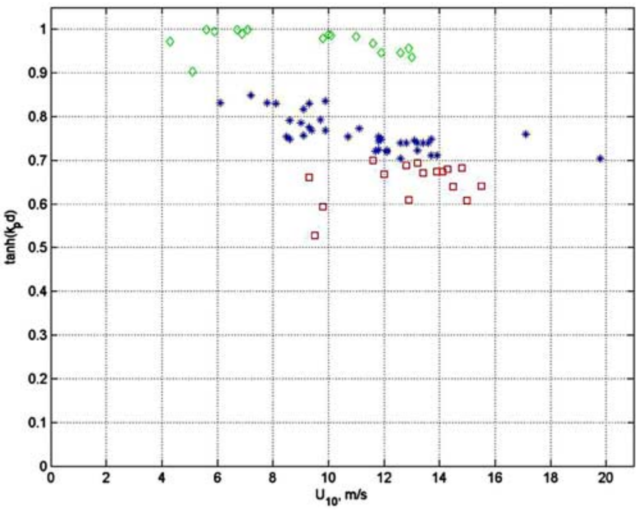

Figure 3. Classification of the Lake George data used. Dimensionless depth parameter tanh(k_pd) versus U_{10} where k_p is peak wave number, d is dimensional water depth. Diamonds are regarded as those corresponding to deep-water waves, asterisks are intermediate depths, squares are shallow water.

dependence on the wind speed, wave age, finite bottom depth, and other ocean and atmosphere parameters.

[33] The WOWC approach can be considered as an alternative to the semi-empirical approach based on the dimensional analysis, which relates aerodynamic roughness of the sea surface to the integral characteristics of the sea state (e.g., significant wave height, wave age, etc.) and the wind speed [e.g., *Drennan et al.*, 2005]. However, the WOWC approach is superior to the semi-empirical approach as it considers the wave spectrum in the full range of wave numbers, beginning from capillaries and ending by long dominant waves and swell, and takes into account peculiarities of interaction of waves with the atmosphere.

[34] The WOWC theory was successfully applied to the open ocean (pure wind sea) [*Kudryavtsev and Makin*, 2001], developing wind seas [*Makin and Kudryavtsev*, 2002; *Guo-Larsen et al.*, 2003], and the laboratory condition [*Makin et al.*, 2004] to explain the observed behavior of the sea drag. The WOWC model explains the wind speed, wave age and finite depth dependences of the sea drag (drag coefficient), and gives a reasonable qualitative agreement with measurements. Thus the WOWC model provides a powerful tool for data interpretation.

[35] In the present paper the model will be used as a reference for measurements. The concise description of the model is made by *Makin and Kudryavtsev* [2003]. The model computes the wind stress τ and therefore C_d, based on knowledge of the measured dominant wave spectrum and the mean wind speed U_{10}.

4. The Data

[36] The only criterion which we used in pre-selecting the data was the requirement for winds to be onshore. The Lake George platform was located close to the eastern shore of the lake, and therefore records of easterly winds were not considered. The wind flow undergoes a complex and poorly understood transformation when crosses from the land into the sea which does not relate to the general problem of sea drag over the ocean studied in the present paper.

[37] For the Lake George results being possible to compare with conclusions of other known studies of sea drag, the data have to be classified, first of all, in terms of the dimensionless water depth and wind-forcing. Proximity of the bottom prohibits development of long waves, and the finite-depth waves can reach their full development and still remain short and stay strongly forced [e.g., *Young and Verhagen*, 1996]. We need to be able to look at those waves and regular deep-water waves separately.

[38] In Figure 3, dimensionless depth parameter tanh(k_pd) is plotted versus U_{10} where k_p is peak wave number, d is dimensional water depth. Diamonds (tanh(k_pd) > 0.9, k_pd > 1.5) will be regarded as deep-water cases, asterisks (0.9 > tanh(k_pd) > 0.7, 1.5 > k_pd > 0.9) as intermediate depths, and squares (tanh(k_pd) < 0.7, k_pd < 0.9) as shallow water records. As will be seen below, the last two groups of data are hardly distinguishable, but physical characteristics of the first group differ. As one can expect, the strongest winds forced the waves into dimensionless shallow or intermediate depths, but the range of wind speeds corresponding to waves found in deep water is still quite broad: U_{10} < 14m/s. We should point out that, according to the traditional classification of waves with respect to depth [e.g., *Young*, 1999], all our records correspond to intermediate depths: $\pi/10 < k_pd < \pi$.

[39] The classification of the data is further analyzed in Figure 4. In the top panel, the wind-forcing parameter U_{10}/c_p is plotted versus U_{10}. Whereas the deep-water diamonds are scattered, the finite-depth data points are all lined up. The enveloping straight line signifies the apparent limit: in the bottom-limited Lake George environments this line indicates the full-development phase speed of $c_p \approx 3$ m/s. In the water of d ~1 m, this speed corresponds to peak frequency of $f_p \approx 0.3$ *Hz*. The deep-water records are therefore quite young waves which have not reached the bottom-limited full development.

[40] The bottom panel of Figure 4 shows steepness of $H_sk_p/2$ where H_s is significant wave height. The steepness is plotted versus U_{10} and it is noticeable that, in circumstances where the downshift of peak frequency is impossible (asterisks and squares), there is a trend and the finite-depth waves on average grow their steepness in response to increasing wind speeds. It is interesting and somewhat unexpected to also note that all the deep water waves are steeper if compared to the bottom-limited waves at the same wind speed. We see two possible explanations for this fact.

[41] The first reason can be an extensive severe breaking of dominant finite-depth waves which reduces their mean height. Indeed, the bottom proximity prevents development of long waves by making them break. In the work of *Manasseh et al.* [2006], record 311823 of present Table 1 was shown to have 100% waves breaking at frequency of 0.8 f_p.

[42] This reason, however, is hypothetical as the breaking rate does not necessarily characterize the breaking severity, i.e., wave energy and height loss, and we do not have information on the severity. Also, the breaking rates for the

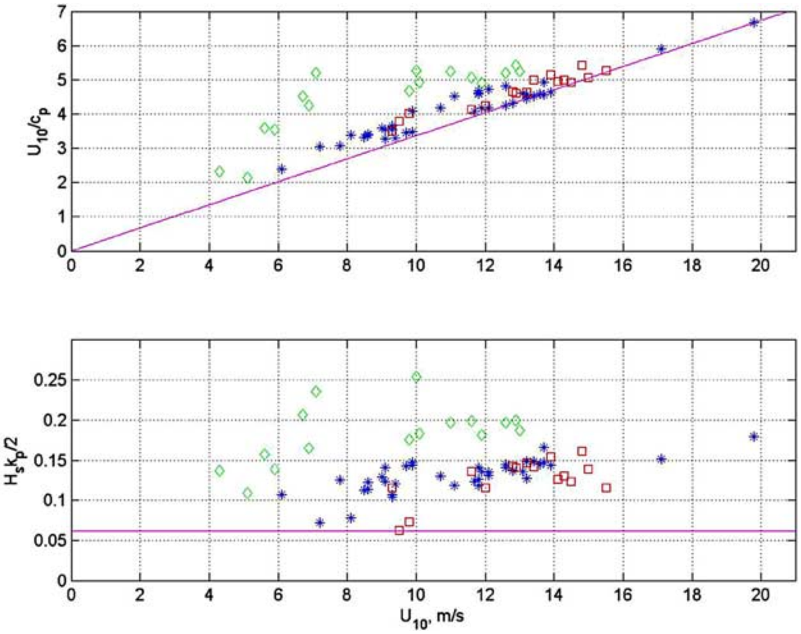

Figure 4. (top panel) Wind-forcing parameter U_{10}/c_p versus U_{10} where c_p is phase speed of peak waves. Symbols are as in Figure 3. The solid line envelope of U_{10}/c_p = 0.34 U_{10} signifies the Lake George bottom-limited full-development phase speed of $c_p \approx 3$ m/s. (bottom panel) Wave steepness $H_s k_p/2$ versus U_{10} where H_s is significant wave height. The solid line shows breaking threshold for dominant waves [*Babanin et al.*, 2001].

deep-water cases plotted in Figure 4, are expected to be in fact even higher if compared to their bottom-limited counterparts. The solid line in the bottom panel shows the breaking threshold for dominant waves inferred from the study of *Babanin et al.* [2001] by assuming that $H_p \approx 0.9\ H_s$ where H_p is the peak wave height obtained by integrating the wave spectrum in $\pm 0.3 f_p$ frequency range. According to *Babanin et al.* [2001], the dominant breaking rates are proportional to the squared difference between peak wave steepness $H_p k_p/2$ and the threshold, and therefore the rates should be greater for the diamond-denoted records. It is worth highlighting that all the Lake George records used in the current analysis have their steepnesses exceeding the breaking threshold and thus dominant waves in all those records were breaking which fact should have further contributed to the sea drag [e.g., *Maat and Makin*, 1992; *Kudryavtsev and Makin*, 2007].

[43] The second, more definite reason is the difference between the shape of deep-water and finite-depth spectra. It may or may not be caused by an extensive breaking severity, but it has been shown that the spectral peaks are relatively flatter for the bottom-limited waves [*Young and Babanin*, 2006].

5. Comparison of the Measurements and the Model

[44] Before comparisons of the experiment and model simulations are conducted, we need to conduct a consistency check of a general behavior of the drag coefficient C_d measured at Lake George in standard terms. In the left panel of Figure 5, C_d is plotted versus U_{10}. Scatter of data points is very large and does not reveal any joint dependence. To some extent, it is surprising that the deep-water data on average do not exhibit the highest drag at a given wind speed as one could expect given the fact that they possess the highest steepness at each U_{10}. For comparison, a selection of C_d-versus-U_{10} dependences by other authors are also shown: bold solid line is after *Donelan* [1982], solid lines are after *Smith* [1980] and *Smith et al.* [1992] (the steeper line), dashed line is after *Large and Pond* [1982], dash-dotted line is after *Yelland and Taylor* [1996], dotted line is after *Geernaert et al.* [1986]. Detailed discussion of these comparisons will be conducted in section 6 below after the definition of the curved envelope will be derived. Overall, we should conclude that the Lake George estimates of sea drag are in quantitative agreement with some of the known field measurements while significantly overvalue the others, particularly at higher wind speeds. The fact that high-gustiness Lake George points at $U_{10} < 10$m/s are above all curves does not contradict this statement as in Lake George low values of the sea drag are absent due to natural reasons whereas they are present in the open-ocean water bodies. This issue is discussed in detail in section 6.

[45] In the right panel, drag coefficient C_d is shown as a function of sea state U_{10}/c_p. Again overall scatter is prohibitively large, but if the deep-water data points are segregated, they exhibit a good correlation with the wind-forcing parameter. As with the wind speed U_{10}, this dependence will be analyzed in detail in section 6, where the meaning of the other curved lines will also be explained. At this stage, we should point out that for the depth-limited data points variation of U_{10}/c_p is the same as variation of U_{10} as the respective phase speeds c_p remain constant.

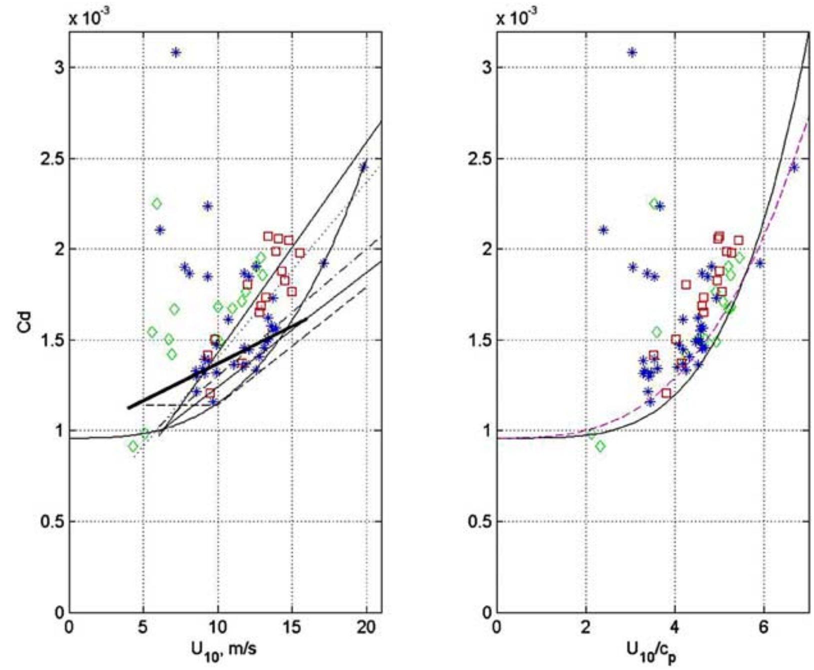

Figure 5. (*left panel*) In both panels, symbols are as in Figure 3. Drag coefficient C_d versus U_{10}. Meaning of the solid curved line is same as of Figure 9b. Selection of C_d-versus-U_{10} dependences by other authors are shown: bold solid line is after *Donelan* [1982], solid lines are after *Smith* [1980] and *Smith et al.* [1992] (the steeper line), dashed line is after *Large and Pond* [1982], dash-dotted line is after *Yelland and Taylor* [1996], dotted line is after *Geernaert et al.* [1986]. (*right panel*) Drag coefficient C_d versus U_{10}/c_p. Meaning of the solid and dashed lines are same as in Figure 9d.

[46] Figure 6 shows comparison of measured and modeled wind stresses for the 74 Lake George records in terms of a scatterplot. Agreement in the mean is good, the regression line lays on the bisector and the correlation coefficient equals 0.95. This agreement points out that the WOWC model, as it is described in section 3, is capable of reproducing the Lake George conditions very well in general, and therefore it is possible to concentrate on details of the differences in order to identify the processes responsible for such differences.

[47] In Figure 7, the comparison is done in terms of the ratio of modeled to measured stress. Overall agreement within 20% for the bulk of the data is quite satisfactory given the variety of physical phenomena, which can alter the field drag and are absent in the model. However, there are clear outliers that the model cannot reproduce. It is interesting to notice that they are not random but represent consequent series of irregular data points: 13–19 correspond to abnormally high peak frequencies, records 24–26 were taken just before the wind suddenly doubled its speed, 61–63 are cases of week-to-moderate gradually growing wind and waves with peak frequency constantly dropping, and it is only point 71 that represents a single outlier.

[48] The outliers are most interesting to analyze. It appears that, if the wind gustiness $G_{detrended} \geq 0.09$, the modeled cases tend to deviate significantly from the measurements. As mentioned above, the present version of the model works was designed for steady-wind conditions and therefore the gustiness has not been included, but apparently played a role in the lake. For example, for the most distant outliers 61, 62, and 71 the gustiness is 0.15, 0.13, and 0.12. The mean wind speed trends can potentially cause a similar result, possibly in different directions. Therefore the param-

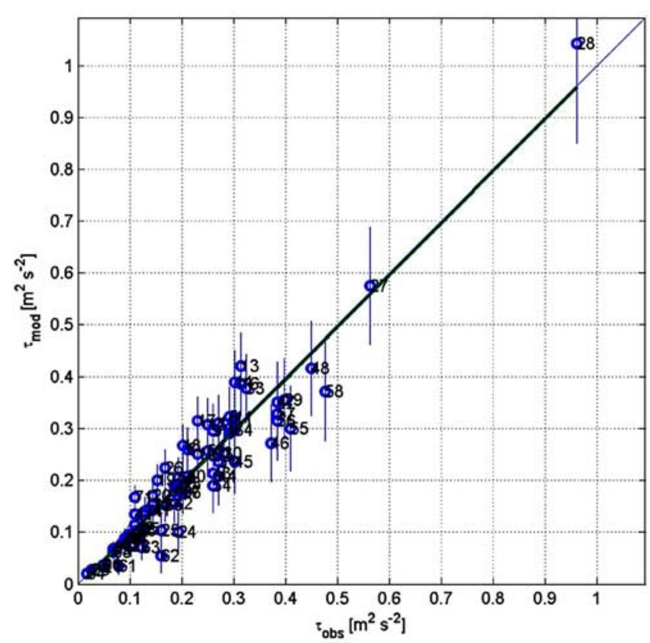

Figure 6. Modeled stress $\tau_{\rm mod}$ versus measured stress τ_{obs}.

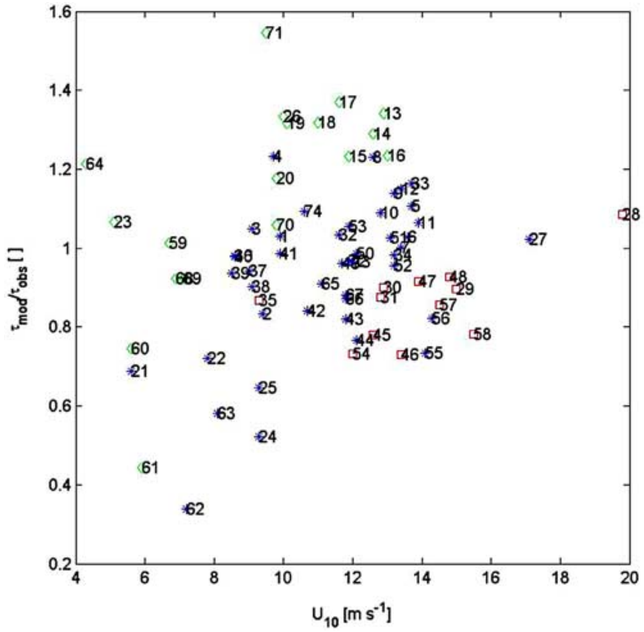

Figure 7. Ratio $\tau_{\mathrm{mod}}/\tau_{obs}$ versus U_{10}.

eterization of sea drag needs a correction for wind trends and gustiness, and these effects need to be scrutinized.

6. Wind Gustiness and Instability

[49] We begin our analysis of effects that wind trend and gustiness have on sea drag by detailing the wind properties first. Dimensional and dimensionless gustiness (see equation (3) above) are plotted in Figures 8a and 8b respectively. As one would expect, dimensional gustiness tends to increase toward stronger winds whereas dimensionless gustiness has the opposite trend, but both trends are quite crude. Largest values of dimensionless gustiness G are exhibited by a set of deep-water cases (diamonds) as those also correspond to the lightest winds. Values of the mean trend T (equation (2)) in our measurements (Figure 8c) were randomly scattered within the range of $T \approx \pm 0.2 \frac{m/s}{\min}$.

[50] Some order in our ability to predict the gustiness is brought about by estimating $G_{detrended}$ rather than G. Since the gustiness can apparently affect the wind stress (sea drag), but is not always measured directly, it would be desirable to have a quantitative dependence of G or $G_{detrended}$ on the mean wind speed as the latter is more readily available.

[51] The detrended gustiness, dimensional and dimensionless, are shown in Figures 8d and 8e respectively. Although scatter of individual data points is still large and it is obviously not possible to unambiguously predict $G_{detrended}$ as a function of U_{10}, it is feasible to identify an upper limit for such gustiness. In dimensional units, it appears to be

$$std(U_{10detrended}) = 0.06 U_{10}^{0.29}, \tag{7}$$

which translates into dependence for dimensionless gustiness:

$$G_{detrended} = 0.60 U_{10}^{-0.71}. \tag{8}$$

[52] The largest reduction of $G_{detrended}$ compared to G occurred for the set of light-wind deep-water cases which in

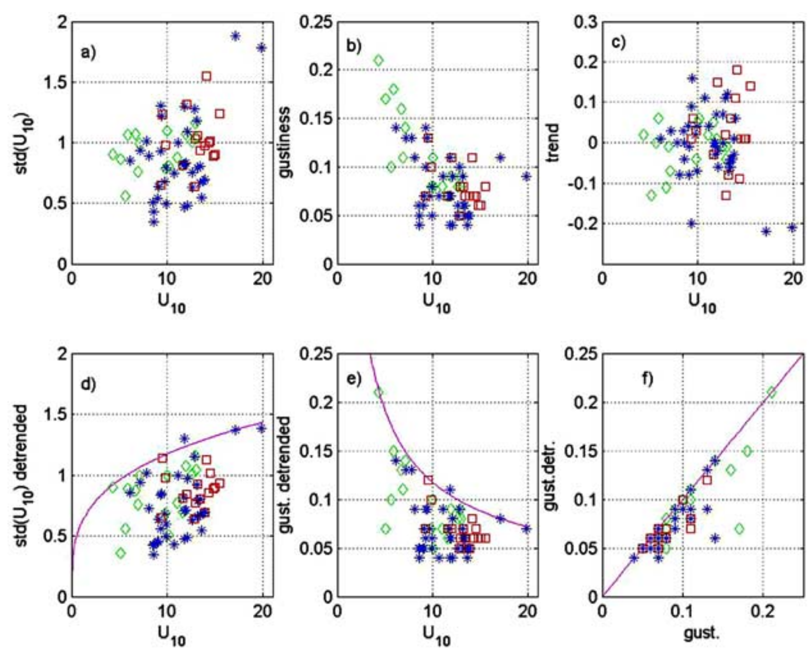

Figure 8. Symbols are as in Figure 3. (a) Dimensional measure of gustiness as $std(U_{10})$ versus U_{10}. (b) Dimensionless measure of gustiness $std(U_{10})/U_{10}$ versus U_{10}. (c) Linear trend T coefficient (2) versus U_{10}. (d) $std(U_{10})$ versus U_{10}, detrended wind records. Solid line is envelope $std(U_{10}) = 0.60U_{10}^{0.29}$. (e) $std(U_{10})/U_{10}$ versus U_{10}, detrended wind records. Solid line is envelope $std(U_{10})/U_{10} = 0.60U_{10}^{-0.71}$. (f) Dimensionless gustiness detrended versus original.

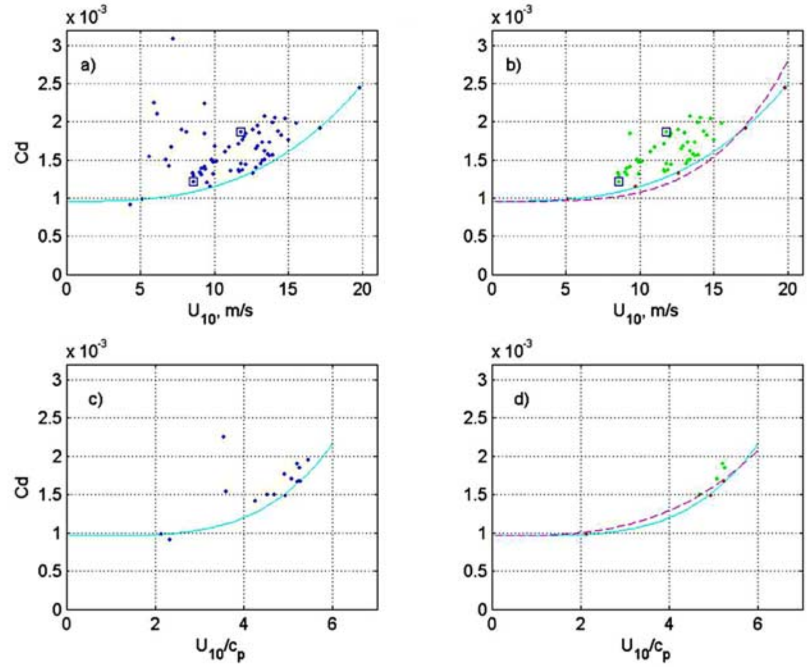

Figure 9. (a) Drag coefficient C_d versus U_{10}. Meaning of the solid line and the squares are same as in Figure 9b. (b) Drag coefficient C_d versus U_{10}, for gustiness $std(U_{10})/U_{10} < 0.09$. Solid line is the lower envelope of $C_d = 1.92 \cdot 10^{-7}\ U_{10}^3 + 0.00096$. Squares denote two points with the lowest measured gustiness of $std(U_{10})/U_{10} = 0.04$ and zero main wind trend. Dashed line is dependence (d) converted using the limiting value of $c_p \approx 3$ m/s. (c) Drag coefficient C_d versus U_{10}/c_p for deep-water records. Meaning of the solid line is same as in *d*). *d*) Drag coefficient C_d versus U_{10}/c_p, for gustiness $std(U_{10})/U_{10} < 0.09$. Solid line is the lower envelope of $C_d = 9.33 \cdot 10^{-7}(U_{10}/c_p)^4 + 0.00096$. Dashed line is dependence *b*) converted using the limiting value of $c_p \approx 3$ m/s.

Figure 8e merged, apart from a single point, with the finite-depth cases. At the other end of the graph, our two strongest-wind cases appear to exhibit the limiting gustiness for given wind speeds. In general, $G_{detrended} \leq G$ as expected (Figure 8f).

6.1. Drag Dependence on Mean Wind Speed

[53] Figures 9 and 10 highlight the main results of current paper as far as the sea drag is concerned. Figure 9a, complete set of C_d versus U_{10}, is our starting point. The data points are the same as those in Figure 5(left) and are replotted here within the same scales as the other subplots in Figures 9 and 10 for convenience of comparisons. The scatter is formidable, particularly for winds $U_{10} < 10$ m/s. Since the modeling showed that the most distant outliers in terms of wind stress were cases of significant gustiness, we now set a limit for $G_{detrended}$ allowed and were gradually reducing this limit in order to see what effect it has on the C_d scatter.

[54] It was found that most obvious outliers were gone by the time we reduced the limit down to $G_{detrended} < 0.09$. The remaining data points are shown in Figure 9b. The scatter is still significant, but it has become of a typical magnitude for C_d-versus-U_{10} data sets which have been historically employed to obtain the sea drag dependences. Further reduction of the limiting value of $G_{detrended}$ did not improve the scatter. It is apparent that the gustiness is not the only phenomenon altering the drag, but impacts of a strong gustiness have an effect on the drag, particularly for low and moderate winds. Therefore finding the limiting value is very encouraging as it provides a ground for preliminary data selection when analyzing C_d dependences.

[55] It is quite possible now to draw a joint dependence through our data points, the result would be closest to the finite-depth North Sea measurements: *Geernaert et al.* [1986] and the HEXOS parameterization of *Smith et al.* [1992] (see Figure 5 left). Dependence of *Donelan* [1982] is also within our data range, but other dependences shown in Figure 5 (left) deviate away from our data. For stronger winds they extend into the range of lower C_d values which are non-existent at Lake George.

[56] As above, it is most informative to analyze the differences rather than agreements. Why *Smith* [1980], *Large and Pond* [1982], and *Yelland and Taylor* [1996], among others, measured the lower magnitudes of C_d which did not occur at Lake George?

[57] It is generally accepted that in finite depths the sea drag is greater than in the open ocean. *Smith et al.* [1992] point out that ‘‘in open-sea conditions the drag coefficient 10–15% lower than in coastal or shallower situations’’. The bottom-limited Lake George measurements certainly support this conclusion.

[58] *Smith et al.* [1992] mention that ‘‘this difference is believed to be due to a difference in typical sea state’’. This difference in sea state, however, can have three separate implications for the sea drag. The first one is due to possible variation of the short-wave roughness (high-frequency

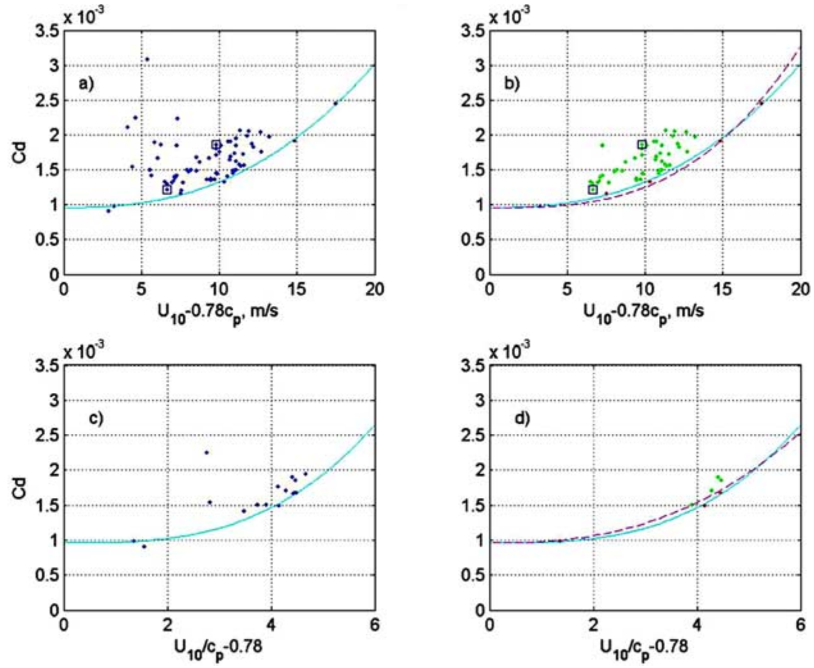

Figure 10. (a) Drag coefficient C_d versus $U_{10} - c_p$. Meaning of the solid line and the squares are same as in Figure 10b. (b) Drag coefficient C_d versus $U_{10} - 0.78c_p$, for gustiness $std(U_{10})/U_{10} < 0.09$. Solid line is the lower envelope of $C_d = 1.155 \cdot 10^{-6}(U_{10} - 0.78c_p)^{5/2} + 0.00096$. Squares denote two points with the lowest measured gustiness of $std(U_{10})/U_{10} = 0.04$ and zero main wind trend. Dashed line is dependence (d) converted using the limiting value of $c_p \approx 3$ m/s. (c) Drag coefficient C_d versus $U_{10}/c_p - 0.78$ for deep-water records. Meaning of the solid line is same as in Figure 10d. (d) Drag coefficient C_d versus $U_{10}/c_p - 0.78$, for gustiness $std(U_{10})/U_{10} < 0.09$. Solid line is the lower envelope of $C_d = 7.83 \cdot 10^{-6}(U_{10}/c_p - 0.78)^3 + 0.00096$. Dashed line is dependence (b) converted using the limiting value of $c_p \approx 3$ m/s.

spectrum level) at different wave development stages. Such variation was indicated by a number of authors. Here, we rely on results of *Babanin and Soloviev* [1998] who showed that the high-frequency level depends on the sea state for mature waves only ($U_{10}/c_p < 1.45$) and remains constant otherwise. Therefore we do not consider this implication, particularly as the spectrum-tail level variations, if were important, would take place both in the North Sea and Lake George. In the North Sea, however, *Geernaert et al.* [1986] and *Smith et al.* [1992] had, for example, occasional values of $C_d < 1.5 \cdot 10^{-3}$ at $U_{10} \sim 15$ m/s which clearly did not happen at Lake George. Therefore the complete lack of low values of sea drag in Lake George is due to a reason which sometimes happen in the sea, but was completely absent in our lake.

[59] This reason is not the RMS wave height which is often expected to be higher at the bottom-limited environment. Effects of the wave height on the sea drag have been suggested [e.g., *Smith et al.*, 1992; *Taylor and Yelland*, 2001; *Oost et al.*, 2001], but they can hardly be linked to the finite-depth drag. First of all, the Lake George deep-water diamonds exhibit dominant steepness higher than the bottom-limited points (Figure 4 bottom), and second of all, their sea drag is not greater (Figure 5 left).

[60] This brings us to the third sea-state dependence implication: absence of long waves at earlier wave development stages. Such stages are more common in the bottom-limited environments and were most common at Lake George where frequencies $f_p < 0.3$ *Hz* were prohibited by the bottom proximity. Also, small size of the lake did not allow for any swell to take place. Lack of long waves signifies absence of possibility for the waves to overrun the wind and, therefore, to give the momentum back to the atmosphere, even if partially. We believe that this fact is responsible for not having the lower C_d values at Lake George where such possibility was missing almost entirely.

[61] Mechanisms, by which the feedback is provided from the waves to the wind, as well as experimental evidences of such feedback, are available in the literature [e.g., *Grachev et al.*, 2003; *Kudryavtsev and Makin*, 2004]. *Lavrenov* [2004] showed that this may result in return energy fluxes from the waves into the atmospheric boundary layer up to a quarter of the total wind-to-wave flux in magnitude. On average, even if the waves across the spectrum keep receiving the momentum from the wind, presence of the outrunning waves would cause a reduction of C_d with respect to the ideal conditions.

[62] If this is true, in the open seas, particularly in the deep ocean in case of mature waves or in presence of swell, we should expect lower value points of the sea drag. In the bottom-limited environments open to the ocean, where long waves cannot develop locally, there will be fewer such points as they would mainly relate to light winds or swell having propagated in from deeper waters (*Geernaert et al.* [1986] and *Smith et al.* [1992] data would satisfy this condition). For the deep-water old seas such points should

be abundant and will cause average magnitudes of C_d and average sea drag dependences to tend toward lower values (*Smith* [1980], *Large and Pond* [1982], *Yelland and Taylor* [1996] results should relate to such circumstances).

[63] In Figure 9b, one can visualize a lower envelope passing through the five bottom points lying on a common line. The best-correlation (99.96%) power law fit to these points gives dependence of

$$C_d = 3.09 \cdot 10^{-7} U_{10}^{2.83} + 0.000953. \qquad (9)$$

[64] Given uncertainties of this empiric match based on 5 points, we found reasonable to replace the fit with a physically more sound cubic parameterization (correlation 99.92%) which occurs if the offset is 0.00096:

$$C_d = 1.92 \cdot 10^{-7} U_{10}^{3} + 0.00096. \qquad (10)$$

[65] Dependence (10) is plotted in Figure 9b as the solid line and is also plotted in Figures 9a and 5(left) for reference.

[66] The lower envelope of Figure 9b provides some Lake George ''ideal'' relationship for the sea drag C_d as a function of wind speed U_{10} and should be regarded as a reference. At this stage, we do not know what set of physical properties at sea defines the ideal conditions. Absence of gustiness and mean wind trend, for example, does not place the data points on the ideal curve. In the figure, squares denote two points with the lowest measured gustiness of $G_{detrended}$ = 0.04 and zero main wind trend. These squares are well within the joint cloud formed by the data after the high-gustiness points were removed.

[67] Any deviation from the ideal conditions, however, causes the drag at Lake George to increase. In the open seas, as has been mentioned above, the deviations can lead the drag to a decrease as well as to the increase.

[68] Unlike other experimental fits to the sea drag dependences (see Figure 5 left), the ideal-condition dependence (10) is a continuous, rather than segmented, curve whose offset is apparently due to the viscous stress at light winds. It is interesting to note that the offset of 0.00096 is the same as that by *Donelan* [1982] dependence:

$$1000 C_d = 0.96 + 0.041 U_{10} \qquad (11)$$

obtained for 4 m/s < U_{10} < 16 m/s.

6.2. Drag Dependence on Sea State

[69] Influence of the sea state on the drag, although was foreshadowed as mentioned in Introduction, has proved elusive. It may be due to the ambiguity of the wave age concept for the air-sea interaction applications. For the wave spectrum analysis, if a self-similar spectral shape is assumed, the sea state can be a single most important parameter which defines all the others. As far as the sea drag is concerned, however, the sea state can have at least three implications as mentioned in section 6.1 above, and perhaps more. Again, as outlined in Introduction, we believe that, since C_d proved to be such a complex property simultaneously responding to a variety of influencing mechanisms, those implication should be gradually singled out and analyzed individually before synthesized back into a joint dependence.

[70] It is useful, therefore, to still consider the general sea state behavior of the drag in traditional terms of inverse wave age U_{10}/c_p to understand where our data stands with respect to other studies. C_d dependence on U_{10}/c_p is demonstrated in the bottom panels of Figure 9.

[71] The overall data set of C_d versus U_{10}/c_p was plotted in Figure 5 (right) and was very scattered except the deep-water points. It is only these deep-water points which are sensible to analyze in terms of wave age in order to compare results with other studies. Variation of the sea state parameter U_{10}/c_p for the bottom-limited Lake George conditions is caused by the wind speed only because the phase speed of those cannot change ($c_p \approx 3$ m/s, Figure 4 top).

[72] Therefore it is only the deep-water data points (diamonds in Figure 5 right) are plotted in Figure 9c. The data outline some average trend for the sea drag to increase towards younger waves. Since we are now aware that the gustiness superposes an artificial scatter on average dependences, in Figure 9d the gusty points were removed ($G_{detrended}$ < 0.09). The trend is now evident and we can state that dependence of C_d on U_{10}/c_p does exist. Following the logic of section 6.1, however, we do not attempt to draw a joint parameterization of this dependence, but instead produce a lower envelope for an ''ideal'' sea-state relationship. Now that the 0.00096 offset is established, straightforward fit to the three bottom points visually lining-up gives:

$$C_d = 1.45 \cdot 10^{-6} \left(U_{10}/c_p\right)^{3.73} + 0.00096. \qquad (12)$$

[73] As before, we replaced this approximation with the closest integral-power law:

$$C_d = 9.33 \cdot 10^{-7} \left(U_{10}/c_p\right)^{4} + 0.00096 \qquad (13)$$

which is shown as solid line in Figure 9d, as well as in Figures 9c and 5(right).

[74] We must emphasize that a fit based on matching a higher-order polynomial term (the offset term is known) to three points only must be exercised with a great caution. We realize that analysis based on (13) has a significant degree of speculation, but we find it necessary in order to at least raise an issue which may or may not eventually lead to overcoming the decades-long stagnation in understanding the sea drag dependences.

[75] Having that in mind, we will see that equations (13) and (10), imply a different dependence of C_d on U_{10}. For the same wave age achieved at different wind speeds, C_d is a cubic function of U_{10}, whereas for the same wind speed along the wave fetch (different wave age), C_d is proportional to $(U_{10}/c_p)^4$. For a given c_p, or if c_p is fixed as it is in finite-depth Lake George records (Figure 4 top), different wind speeds will formally create variation of the sea state conditions, but variation of the sea drag will be proportional to $(U_{10}/c_p)^3$ rather than to $(U_{10}/c_p)^4$.

[76] In Figure 9d, dependence (10), converted into a U_{10}/c_p-dependence by means of the limiting value of $c_p \approx 3$ m/s, is plotted as dashed line. The differences in terms of C_d are not large, but obvious, and their implications are best discussed with the use of Figure 5 (right) where the bulk

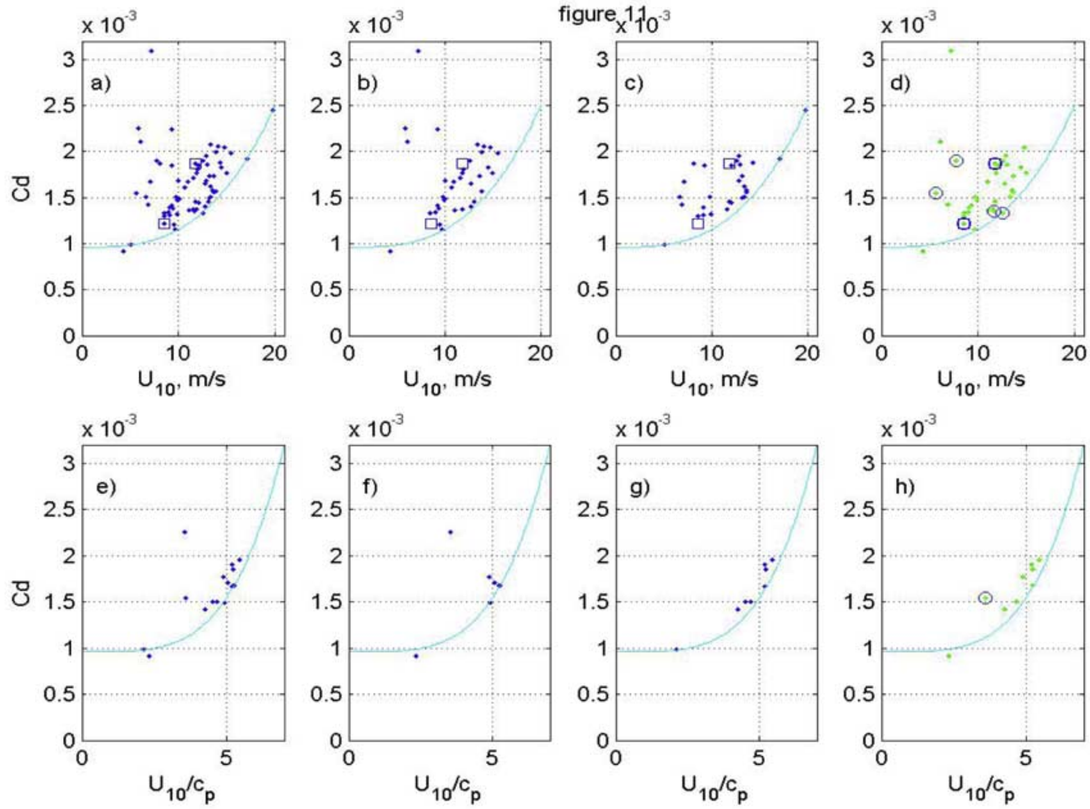

Figure 11. (top panels) Drag coefficient C_d versus U_{10}. Solid line is the lower envelope of $C_d = 1.92 \cdot 10^{-7} U_{10}^{3} + 0.00096$ from Figure 9b. Squares denote two points with the lowest measured gustiness of $std(U_{10})/U_{10} = 0.04$ and zero main wind trend. (a) All data points. (b) Positive trend. (c) Negative trend. (d) Absolute value of the trend slope $abs(trend) < 0.05$. Zero trend records are circled. (*bottom panels*) Drag coefficient C_d versus U_{10}/c_p for deep-water records. Solid line is the lower envelope of $C_d = 9.33 \cdot 10^{-7}(U_{10}/c_p)^4 + 0.00096$ from Figure 9d. (e) All data points. (f) Positive trend. (g) Negative trend. (h) Absolute value of the trend slope $abs(trend) < 0.05$. Zero trend records are circled.

of data is plotted in a C_d-versus-U_{10}/c_p graph. It is seen that three points in the bulk plot are below the ideal wave-age dependence. The two strong-wind points are worth attention. They are bottom-limited and therefore variation of the sea drag for them is described by the $(U_{10}/c_p)^3$ dependence. As a result, values of C_d at $U_{10}/c_p > 5.56$ are reduced below the ideal wave-age line.

[77] Back to Figure 9b, the parameterization (13) is converted into a C_d-versus-U_{10} dependence and shown as dashed line. Intersection of the two curves occurs at $U_{10} \cong 16.7$ m/ s. What can this imply for the complexity of ocean situations? Scatter. For a given wind speed, if measurements of C_d are conducted at different sea states, values of C_d can turn different even if all the other properties are ideal. Minimal scatter, caused by this particular reason, would be expected at wind speeds of $U_{10} \cong 15 \div 18$ m/s. Further experiments and modeling is needed to quantify, and in fact to verify this conclusion, but our inspection of published data indicate a possible reduction of the scatter at these wind speeds, if obvious outliers are filtered out: in Figure 6 of *Smith* [1980], Figure 3 of *Large and Pond* [1982], Figure 5 of *Geernaert et al.* [1986], Figures 7 and 9 of *Smith et al.* [1992].

[78] Following the discussion of the sections 6.1 and 6.2, some modifications to the original C_d dependences may be needed. If the sea drag is affected by the fast waves in a serious way, as described above, extrapolation of the dependences obtained for slow waves into $U_{10}/c_p < 1$ conditions may not be correct. Mechanisms of the wave-to-wind momentum return may be quite different to those which are responsible for the wind-to-wave input, and therefore a mere changing the sign will not necessarily work. Can the sea drag be negative? The extrapolations will not produce that and generally speaking may not be able to accommodate any of the $U_{10}/c_p < 1$-specific conditions. Therefore we found it reasonable to also offer the sea drag dependences which asymptote to $U_{10} \cong 0.78\ c_p$ rather than to $U_{10} \cong 0$. $U_{10}/c_p = 0.78$ is the Pierson-Moscowitz sea-state limit, which may be controlled by the balance of negative and positive wind-wave fluxes, and thus it was preferred to the $U_{10}/c_p = 1$ condition. The latter is only an approximate constraint as the choice of 10m reference height is quite artificial.

[79] In Figure 10, data of Figure 9 are replotted in terms of $U_{10} - 0.78\ c_p$ and $U_{10}/c_p - 0.78$. Overall scatter in subplots *a* and *c* did not change noticeably, and perhaps slightly improved in panel *b* for data points with gustiness $G_{detrended} < 0.09$. The solid lined ideal approximations are

$$C_d = 1.155 \cdot 10^{-6}\left(U_{10} - 0.78c_p\right)^{5/2} + 0.00096 \qquad (14)$$

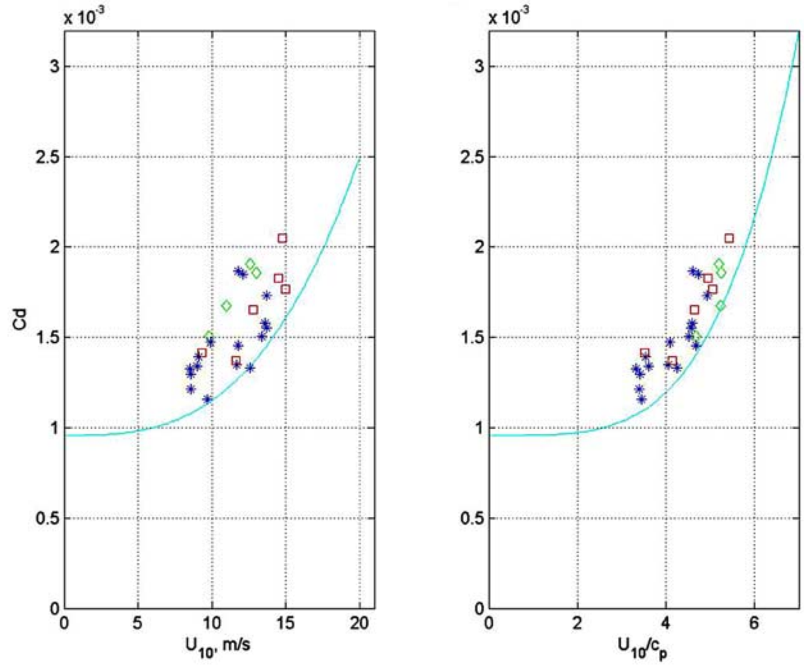

Figure 12. (*left panel*) Drag coefficient C_d versus U_{10}. (*right panel*) Drag coefficient C_d versus U_{10}/c_p. For both panels, gustiness $std(U_{10})/U_{10} < 0.09$, absolute value of the trend slope $abs(trend) < 0.05$. Symbols are as in Figure 3, solid-line dependences are as in Figure 9.

in the top panels and

$$C_d = 7.83 \cdot 10^{-6}\left(U_{10}/c_p - 0.78\right)^3 + 0.00096 \qquad (15)$$

in the bottom panels. As above, the closest physically sound exponents of 5/2 and 3 were preferred to the direct statistical fits which provided exponents of 2.42 and 2.80 respectively. Intersections of the dash-lined converted dependences with the ideal solid lines occurred at $U_{10} - 0.78\ c_p = 15.85$ m/s in Figure 10b and at $U_{10}/c_p - 0.78 = 5.28$ in Figure 10d.

6.3. Influence of the Mean Wind Trend

[80] Importance of the wind trends in terms of sea drag C_d appears to be much less significant than that of the gustiness. The wind trend T effects are analyzed in Figure 11 where symbols and solid lines of Figure 9 are retained.

[81] In Figure 11a, complete set of C_d-versus-U_{10} data points are replotted within the same scales as the other subplots in this figure for convenience of comparisons. Values of the trend are broadly scattered in the range of $T \approx \pm 0.2\ \frac{m/s}{\min}$ (Figure 8c), and we started our analysis from separating positive (Figure 11b) and negative (Figure 11c) trends. Both trends occurred in a broad range of wind speeds which fact allowed us to qualitatively compare the two data sets. Scatter which correspond to $T > 0$ is much higher compared to that of $T < 0$. Since the most distant outliers were correlated with the gustiness, it means that gustiness of slowly increasing winds at Lake George was greater compared to the slowly decaying winds. Points of zero trend and minimal (0.04) gustiness are also indicated (squares) and do not appear to be asymptotic values of the raising or falling winds which clearly indicate a contribution of other than wind instability factors to the sea drag.

[82] To further detail effects of the wind trend, C_d at most stable mean wind conditions ($T < |0.05|\frac{m/s}{\min}$) are plotted in Figure 11d. It is quite obvious that most of the scatter seen earlier was not caused by the wind trends as even the zero-trend points (circles) appear as both most distant outliers and points closest to the ideal-condition curve.

[83] An analogous set of four plots, with drag coefficient C_d versus U_{10}/c_p for deep-water records, is shown in the bottom panels of Figure 11. Conclusions with respect to the mean-wind trend effects on the wave age dependences are quite the same as above. We should perhaps point out that for the decreasing winds all our data points line up closely along the ideal-condition dependence. Given the limited amount of Lake George deep-water data, however, we will refrain from concluding that slowly decaying winds are those associated with the ideal drag dependence on sea state until further verifications.

7. Discussion and Conclusions

[84] As mentioned above, the issue of the sea drag C_d dependences on wind speed U_{10} and sea state U_{10}/c_p is decades-long with little progress in terms of improvement of the scatter since almost the 70s. On the basis of accumulated knowledge, we believe that recognition of a new approach to the problem is needed. C_d does increase, on average, once the wind goes up but it is not a simple function of mean wind speed and, therefore, attempts to parameterize it in terms of U_{10} or sea state U/c_p are bound to have a great scatter, no matter how extensive and how precise are the measurements of wind and waves.

[85] In the present paper, we suggest a complex approach to tackle the problem. In short, it is based on recognition of the complex nature of air-sea interaction at small scales,

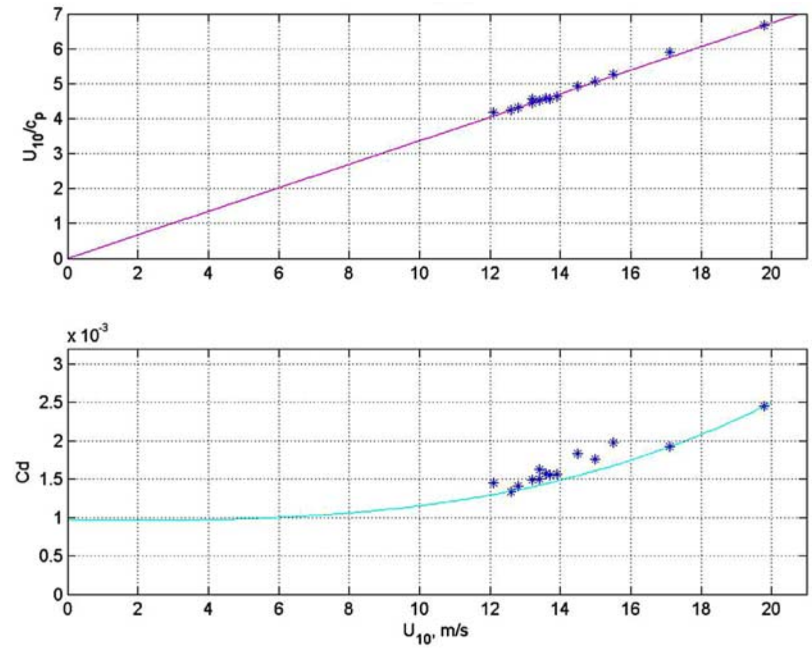

Figure 13. Investigating variation of sea drag C_d due to wind speed U_{10} for fully developed waves. (*top panel*) As in Figure 4, top panel. Only points with deviation less than 1% from the limiting full-development line are chosen. (*bottom panel*) C_d versus U_{10} for these points, solid-line dependence is as in Figure 9b.

where multiple mechanisms affect and alter the sea drag simultaneously, sometimes in opposite directions. In Introduction, we list 16 features which can influence the drag, and perhaps this list is not exhaustive. We believe that this is an underlying reason for the observed large scatter of C_d data. Adopting this perspective, we should be eventually able to significantly reduce the scatter of C_d parameterizations. The contributing mechanisms need to be singled out, studied separately, evaluated and then reunited in a joint parameterization for C_d. An analytical approach should be applied to the mechanisms, wherever it is possible. This will enhance our understanding of their physics to create a complete picture of the complex phenomenon and to produce a general parameterization.

[86] In this regard, we would call on the air-sea interaction community, who have sea drag data, to verify assumptions and conclusions of the present paper. The Lake George data set is substantial, but by far not comprehensive. In particular, it would be most interesting to check whether our limiting envelopes are applicable in water bodies other than Lake George if C_d data for younger seas are separated from their mature-wave-age counterparts, and how general is our $G_{detrended} < 0.09$ limiter in filtering out obvious drag-dependence outliers.

[87] The key feature of our approach is the use of the air-sea interaction WOWC model. The model supplements the experimental investigations with theoretical analysis and, most importantly, allows to isolate and study different effects separately. Comparisons of the experiment with the modeling, and testing the model's capabilities were another primary aim of this paper.

[88] In the process, we have learnt the strengths and weaknesses of the approach which will serve for the continuing studies. Here, we would like to summarize highlights of the present paper.

[89] 1) Overall agreement of the model to predict wind stresses for Lake George conditions is quite good, within 20% for the bulk of the data. This allows to further use the model as an analytical instrument of the study.

[90] 2) Analysis, based on comparisons of the model and experiment, revealed that the most distant outliers were field cases with high wind gustiness G (equation (3)). Setting a limit of $G_{detrended} < 0.09$ as a basis for preliminary data selection allowed us to filter out evident outliers of the sea drag C_d dependences on wind speed U_{10} and sea state U_{10}/c_p (Figure 9).

[91] 3) Once the obvious outliers are removed, some crude dependences of C_d on U_{10} and U_{10}/c_p emerge. These dependences are in approximate agreement with some of other known field parameterizations. The remaining C_d scatter, however, appears to be brought about by causes other than the wind instabilities only and does not asymptote to cases of the zero trend T (equation (2)) and minimal gustiness G (equation (3)). In the two subplots of Figure 12, C_d versus U_{10} and C_d versus U_{10}/c_p are plotted for low values of both T (*abs(T)* < 0.05) and G ($G_{detrended} < 0.09$). Majority of points are still well above the lower envelopes. This means that there is a number of effects contributing to the sea drag, other than gustiness and mean wind trend.

[92] 4) The lower envelopes are an important result of the present paper (equations (10) and (13)). They provide some Lake George "ideal" relationships for the sea drag. At this stage, we do not know what physical properties constitute the ideal conditions. However, almost any deviation from such conditions, at a given wind speed U_{10}, causes the drag at Lake George to increase. We suggest that decrease of the

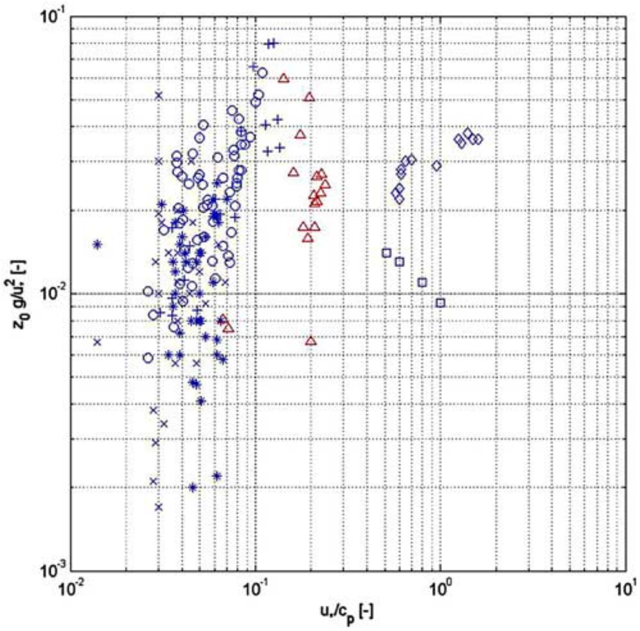

Figure 14. Charnock parameter $z_0 g/u_*^2$ versus inverse wave age u_*/c_p. Symbols indicate data. Circles: HEXMAX [*Janssen*, 1997]; pluses: Lake Ontario; stars: Atlantic Ocean, long fetch; x-marks: Atlantic Ocean, limited fetch [*Donelan et al.*, 1993]; diamonds: wave tank [*Donelan*, 1990]; squares: wave tank [*Keller et al.*, 1992]. Data are compiled from *Donelan et al.* [1993], their Figure 2. Triangles: present paper.

drag with respect to the ideal conditions, which exhibits itself in a number of known open ocean data sets, would be caused by a momentum flux back from the waves to the wind due to long waves outrunning the wind.

[93] 5) For the C_d-versus-U_{10}/c_p dependence, decrease of the drag with respect to the ideal conditions also reveals itself at strong winds where variation of the sea state is achieved due to varying wind speed only (phase speeds of c_p > 3 m/s were not possible in the finite-depth Lake George). We argue (section 6.2) that this is caused by the fact that, for the same wave age achieved at different wind speeds, C_d is a cubic function of U_{10} (10), whereas for the same wind speed along the wave fetch (different wave age), C_d is proportional to $(U_{10}/c_p)^4$ (13).

[94] In this regard it is interesting to look at variation of sea drag C_d due to wind speed U_{10} only, for waves fully developed at the bottom-limited environment. In Figure 13 (top) our selection of data points for this purpose is shown. They are points with deviation less than 1% from the limiting full-development line of $c_p \approx 3$ m/s. In the bottom panel of Figure 13, C_d for these data is plotted versus U_{10}. Overall, such points are quite close to the ideal dependence of C_d on U_{10}, but evidently the deviations are significant. This, once again, signifies a complex nature of the sea drag. Even for such refined selection of conditions, where one could expect C_d to be dependent solely on U_{10}, underlying processes affect and scatter the drag.

[95] 6) The Lake George data set, in terms of wave-age conditions, occupies a niche between the typical ocean and laboratory measurements. It gives us an opportunity to bridge some other air-sea interaction properties of interest. One of the most important of them is the Charnock parameter. In Figure 14, the measured Charnock parameter for deep water points only is plotted versus the sea state parameter in terms of friction velocity u_*. Apart from the lowest point, which is point 71 and most probably is an outlier, the present measurements seem to confirm the general trend of the Charnock parameter as a function of the inverse wave age: it increases with the increase of the inverse wave age parameter, levels off at u_*/c_p of about 0.15 and then decreases again for the laboratory conditions.

[96] Other, perhaps less important, but useful results, should also be mentioned here among conclusions.

[97] 7) Quasi deep-water conditions in finite-depth environments, where spectral peak can still evolve as the waves propagate, associate with dimensionless water depths of ($k_p d > 1.5$, $\tanh(k_p d) > 0.9$). At shallower depths, downshift of the spectral peak is arrested by bottom proximity (Figure 4).

[98] 8) In the quasi-deep-water conditions, the waves are on average steeper compared to those bottom-limited (Figure 4), but their sea drag is not on average greater (Figure 5).

[99] 9) If measurements of the wind gustiness are unavailable, their upper limits at a given wind speed can be estimated by means of equations (7) and (8).

[100] 10) Since extrapolation of the dependences obtained for slow waves into $U_{10}/c_p < 1$ conditions may not be correct, an alternative set of sea drag C_d dependences, which asymptote to the Pierson-Moscowitz value of $U_{10}/c_p = 0.78$ are suggested (equations (14) and (15)).

[101] 11) Effects of slow wind trends ($T < |0.2|\frac{m/s}{\min}$) on the sea drag appear to be small.

References

Agnon, Y., A. V. Babanin, I. R. Young, and D. Chalikov (2005), Fine scale inhomogeneity of wind-wave energy input, skewness and asymmetry, *Geophys. Res. Lett.*, *32*(12), L12603, doi:10.1029/2005GL022701.

Babanin, A. V., and Yu. P. Soloviev (1998), Field investigation of transformation of the wind wave frequency spectrum with fetch and the stage of development, *J. Phys. Oceanogr.*, *28*, 563–576.

Babanin, A. V., I. R. Young, and M. L. Banner (2001), Breaking probabilities for dominant surface waves on water of finite constant depth, *J. Geophys. Res.*, *106*(C6), 11,659–11,676.

Babanin, A. V., I. R. Young, and H. Mirfenderesk (2005), Field and laboratory measurements of wave-bottom interaction, in *Proc. 17th Australasian Coastal and Ocean Engineering Conference and the 10th Australasian Port and Harbour Conference, 20–23 September 2005, Adelaide, South Australia*, edited by M. Townsend and D. Walker, 293–298.

Belcher, S. E., and J. C. R. Hunt (1993), Turbulent shear flow over slowly moving waves, *J. Fluid Mech.*, *251*, 109–148.

Bye, J. A. T., and A. D. Jenkins (2006), Drag coefficient reduction at very high wind speeds, *J. Geophys. Res.*, *111*, C03024, doi:10.1029/2005JC003114.

Dobson, F. W., S. D. Smith, and R. J. Anderson (1994), Measuring the relationship between wind stress and sea state in the open ocean in the presence of swell, *Atmos. Ocean*, *32*, 237–256.

Donelan, M. A. (1982), The dependence of the aerodynamic drag coefficient on wave parameters, In *Proc. First Int. Conf. on the Meteorology and Air-Sea Interaction in Coastal Zone*, Hague, The Netherlands, *Am. Meteorol. Soc.*, 381–387.

Donelan, M. A. (1990), Air-sea interaction in, *The Sea: Ocean Eng. Sci.*, *9*, 239–292.

Donelan, M. A., F. W. Dobson, S. D. Smith, and R. J. Anderson (1993), On the dependence of sea roughness on wave development, *J. Phys. Oceanogr.*, *23*, 2143–2149.

Donelan, M. A., W. M. Drennan, and K. B. Katsaros (1997), The air-sea momentum flux in conditions of wind sea and swell, *J. Phys. Oceanogr.*, *27*, 2087–2099.

Donelan, M. A., B. K. Haus, N. Reul, W. J. Plant, M. Stiassnie, H. C. Graber, O. B. Brown, and E. S. Saltzman (2004), On the limiting aerodynamic roughness of the ocean in very strong winds, *Geophys. Res. Lett.*, *31*, L18306, doi:10.1029/2004GL019460.

Donelan, M. A., A. V. Babanin, I. R. Young, and M. L. Banner (2006), Wave follower measurements of the wind input spectral function. Part 2. Parameterization of the wind input, *J. Phys. Oceanogr.*, *36*, 1672–1688.

Drennan, W. M., H. C. Graber, and M. A. Donelan (1999), Evidence for the effects of swell and unsteady winds on marine wind stress, *J. Phys. Oceanogr.*, *29*, 1853–1864.

Drennan, W. M., H. C. Graber, D. Hauser, and C. Quentin (2003), On the wave age dependence of wind stress over pure wind seas, *J. Geophys. Res.*, *108*(C3), 8062, doi:10.1029/2000JC000715.

Drennan, W. M., P. K. Taylor, and M. J. Yelland (2005), Parameterizing the sea surface roughness, *J. Phys. Oceanogr.*, *35*, 835–848.

Geernaert, G. L., K. B. Katsaros, and K. Richter (1986), Variation of the drag coefficient and its dependence on sea state, *J. Geophys. Res.*, *91*(C6), 7667–7679.

Grachev, A. A., C. W. Fairall, J. E. Hare, J. B. Edson, and S. D. Miller (2003), Wind stress vector over ocean waves, *J. Phys. Oceanogr.*, *33*, 1429–2408.

Guo-Larsen, X., V. K. Makin, and A. S. Smedman (2003), Impact of waves on the sea drag: Measurements in the Baltic Sea and a model interpretation, *The Glob. Atmos. Ocean. Syst.*, *9*, 97–120.

Hara, T., and S. E. Belcher (2002), Wind forcing in the equilibrium range of wind-wave spectra, *J. Fluid Mech.*, *470*, 223–245.

Janssen, P. A. E. M. (1986), On the effects of gustiness on wave growth, *KNMI Afdeling Oceanografisch Onderzoek memo*, 00-86-18, DeBilt, 17 pp.

Janssen, J. A. M. (1997), Does wind stress depend on sea-state or not? - A statistical error analysis of HEXMAX data, *Boundary Layer Meteorol.*, *83*, 479–503.

Keller, M. R., W. C. Keller, and W. J. Plant (1992), A wave tank study of the determination of X-band cross sections on wind speed and water temperature, *J. Geophys. Res.*, *97*, 5771–5792.

Komen, G. I. (1994), Sea surface winds and atmospheric circulation, in *Dynamics and Modelling of Ocean Waves* by G. I. Komen, L. Cavaleri, M. Donelan, K. Hasselmann, S. Hasselmann, and P. A. E. M. Janssen, Cambridge Univ. Press, 48–60.

Kudryavtsev, V. N. (2006), On the effect of sea drops on the atmospheric boundary layer, *J. Geophys. Res.*, *111*, C07020, doi:10.1029/2005JC002970.

Kudryavtsev, V. N., and V. K. Makin (2001), The impact of air-flow separation on the drag of the sea surface, *Boundary Layer Meteorol.*, *98*, 155–171.

Kudryavtsev, V. N., and V. K. Makin (2002), Coupled dynamics of short wind waves and the air flow over long surface waves, *J. Geophys. Res.*, *107*(C12), 3209, doi:10.1029/2001JC001251.

Kudryavtsev, V. N., and V. K. Makin (2004), Impact of swell on the marine atmospheric boundary layer, *J. Phys. Oceanogr.*, *34*, 934–949.

Kudryavtsev, V. N., and V. K. Makin (2007), Aerodynamic roughness of the sea surface at high winds, *Boundary Layer Meteorol.*, doi:10.1007/s10546-007-9184-7.

Kudryavtsev, V. N., V. K. Makin, and B. Chapron (1999), Coupled sea surface atmosphere model. 2. Spectrum of short wind waves, *J. Geophys. Res.*, *104*, 7625–7639.

Large, W. G., and S. Pond (1982), Sensible and latent heat flux measurements over the ocean, *J. Phys. Oceanogr.*, *12*, 464–482.

Lavrenov, I. V. (2004), Weak turbulent fluxes estimation in surface water wave spectrum, in *Proceedings of the* 8th *International Workshop on Wave Hindcasting & Forecasting*, *Hawaii*, *November 14–19, 2004*, 14 pp.

Maat, N., and V. K. Makin (1992), Numerical simulation of air flow over breaking waves, *Boundary Layer Meteorol.*, *60*, 77–93.

Makin, V. K. (1988), Effect of wave interactions in the seawater-adjoining atmospheric boundary layer on flow of energy to wind waves., *Soviet Physics. A Translation of the Physics Section of the Proceedings of the Academy of Sciences of the USSR*, *299*, 276–279.

Makin, V. K. (2005), A note on drag of the sea surface at hurricane winds, *Boundary Layer Meteorol.*, *115*, 169–176.

Makin, V. K., and V. N. Kudryavtsev (1999), Dynamical coupling of surface waves with the atmosphere, in *Air-Sea Exchange: Physics, Chemistry and Dynamics*, edited by G. L. Geernaert, Kluwer Acad. Publ., 73–126.

Makin, V. K., and V. N. Kudryavtsev (2002), Impact of dominant waves on sea drag, *Boundary Layer Meteorol.*, *103*, 83–99.

Makin, V. K., and V. N. Kudryavtsev (2003), Wind-over-waves coupling, in *Wind Over Waves* II, edited by S. G. Sajjadi and J. C. R. Hunt, Horwood Publishing Limited, England, 46–56.

Makin, V. K., V. N. Kudryavtsev, and C. Mastenbroek (1995), Drag of the sea surface, *Boundary Layer Meteorol.*, *73*, 159–182.

Makin, V. K., G. Caulliez, and V. N. Kudryavtsev (2004), Drag of the water surface at limited fetch: laboratory measurements and modelling, in *Geophysical Research Abstracts*, *6*, EGU04-A-00113, EGU General Assembly, April 25–31, 2004, Nice, France.

Makin, V. K., H. Branger, W. L. Peirson, and J. P. Giovanangeli (2007), Stress above wind plus paddle waves: Modelling of a laboratory experiment, *J. Phys. Oceanogr.*, in press.

Manasseh, R., A. V. Babanin, C. Forbes, K. Rickards, I. Bobevski, and A. Ooi (2006), Passive acoustic determination of wave-breaking events and their severity across the spectrum, *J. Atmos. Oceanic Technol.*, *23*, 599–618.

Miles, J., and G. Ierley (1998), Surface-wave generation by gusty wind, *J. Fluid Mech.*, *357*, 21–28.

Oost, W. A., G. J. Komen, C. M. J. Jacobs, C. van Oort (2001), New evidence for a relation between wind stress and wave age from measurements during ASGAMAGE, *Preprint 2001-05 Koninklijk Ned. Meteorol. Inst. (KNMI)*, De Bilt, Netherlands, 30 pp.

Powel, M. D., P. J. Vickery, and T. A. Reinhold (2003), Reduced drag coefficient for high wind speeds in tropical cyclones, *Nature*, *422*, 279–283.

Skafel, M. G., and M. A. Donelan (1997), Laboratory measurements of stress modulation by wave groups, *Geophysica*, *33*, 9–14.

Smedman, A.-S., Hogstrom, H. Bergstrom, A. Rutgersson, K. K. Kahma, and H. Pettersson (1999), A case study of air-sea interaction during swell conditions, *J. Geophys. Res.*, *104*, 25,833–25,851.

Smith, S. D. (1980), Wind stress and heat flux over the ocean in gale force winds, *J. Phys. Oceanogr.*, *10*, 709–726.

Smith, S. D., R. J. Anderson, W. A. Oost, C. Kraan, N. Maat, J. DeCosmo, K. B. Katsaros, K. L. Davidson, K. Bumke, L. Hasse, and H. M. Chadwick (1992), Sea surface wind stress and drag coefficients: The HEXOS results, *Boundary Layer Meteorol.*, *60*, 109–142.

Stewart, R. W. (1974), The air-sea momentum exchange, *Boundary Layer Meteorol.*, *6*, 151–167.

Taylor, P. K., and M. J. Yelland (2001), The dependence of sea surface roughness on the height and steepness of the waves, *J. Phys. Oceanogr.*, *31*, 572–590.

Uz, B. M., M. A. Donelan, T. Hara, and E. J. Bock (2002), Laboratory studies of wind stress over surface waves, *Boundary Layer Meteorol.*, *102*, 301–331.

Vakhguelt, A. (2007), Mathematical model of interaction between finite amplitude wave and the liquid particles, *Proceedings of the 1*8th *Australasian Coastal and Ocean Engineering Conference and the 11th Australasian Port and Harbour Conference, 18–20 July 2007*, *Melbourne, Victoria*, paper 197, 6 pp.

Yelland, M. J., and P. K. Taylor (1996), Wind stress measurements from the open ocean, *J. Phys. Oceanogr.*, *26*, 541–558.

Yelland, M. J., B. I. Moat, P. K. Taylor, R. W. Pascal, J. Hutchings, and V. C. Cornell (1998), Wind stress measurements from the open ocean corrected for airflow distortion by the ship, *J. Phys. Oceanogr.*, *28*, 1511–1526.

Young, I. R. (1999), *Wind generated ocean waves*, Elsevier, 288 pp.

Young, I. R., and A. V. Babanin (2006), The form of the asymptotic depth-limited wind wave frequency spectrum, *J. Geophys. Res.*, *111*, C06031, doi:10.1029/2005JC003398.

Young, I. R., and L. A. Verhagen (1996), The growth of fetch limited waves in water of finite depth. Part I: Total energy and peak frequency, *Coastal Eng.*, *28*, 47–78.

Young, I. R., M. L. Banner, M. A. Donelan, A. V. Babanin, W. K. Melville, F. Veron, and C. McCormick (2005), An integrated system for the study of wind wave source terms in finite depth water, *J. Atmos. Oceanic Technol.*, *22*, 814–828.

A. V. Babanin, Faculty of Engineering and Industrial Sciences, Swinburne University of Technology, Melbourne, Victoria, Australia. (ababanin@swin.edu.au)

V. K. Makin, Royal Netherlands Meteorological Institute (KNMI), De Bilt, Netherlands.